Generalization and Expansion of the Hermia Model for a Better Understanding of Membrane Fouling

Gustavo Dias Pereira *, Lucio Cardozo Filho, Veeriah Jegatheesan *, Reginaldo Guirardello

Posted Date: 5 January 2023

doi: 10.20944/preprints202206.0187.v2

Keywords: Membrane fouling; Hermia model; Fouling model; Pore blocking; Blocking mechanism

Article

Generalization and Expansion of the Hermia Model for a Better Understanding of Membrane Fouling

Gustavo Pereira [1,*], Lucio Cardozo-Filho [1,2], Veeriah Jegatheesan [2] and Reginaldo Guirardello [3]

[1] Department of Chemical Engineering, State University of Maringa, Maringa, Brazil
[2] School of Engineering and Water: Effective Technologies and Tools (WETT) Research Centre, RMIT University, Melbourne, VIC 3000, Australia
[3] College of Chemical Engineering, State University of Campinas, Campinas, Brazil
* Correspondence: gldpereira2@gmail.com; Tel.: +55 44 99182 8901

Abstract: One of the most broadly used models for membrane fouling is the Hermia model, which separates this phenomenon into four blocking mechanisms, each with an associated parameter n. These mechanisms are complete blocking (n=2), intermediate blocking (n=1), standard blocking (n=3/2), and cake formation (n=3/2). The original model, which was obtained through experimental data, is given by an Ordinary Differential Equation (ODE) dependent on n. At the time, this ODE was only solved for these four values of n, which limits the effectiveness of the model when adjusted to experimental data. This paper aims to not only mathematically prove the original Hermia model but also to broaden the scope of this model for any real number n by using the original ODE, the equations of fluid mechanics, and the properties of single and multivariable calculus. The extended Hermia model (EHM) is given by a power law for any n≠2 and is given by an exponential function at n=2. To better test the model, we have performed the model fitting of the EHM and compared its performance to the original four pore-blocking mechanisms in 6 micro- and ultrafiltration examples. In all examples, the EHM performed consistently better than the four original pore-blocking mechanisms. Changes in the blocking mechanisms concerning transmembrane pressure (TMP), crossflow rate (CFR), crossflow velocity (CFV), membrane composition, and pretreatments are also discussed.

Keywords: membrane fouling; hermia model; fouling model; pore blocking; blocking mechanism

1. Introduction

One of the most widely used models to predict membrane fouling is the Hermia model [1]. In the 1982 paper, Hermia was able to frame mathematically the relationship between the accumulated volume and time from experimental data, arriving at the differential equation presented in Eq. 1. Since this model was derived for non-Newtonian fluids, the parameters n and k help to adjust the model for different types of fluids and blocking mechanisms. The original ordinary differential equation (ODE) was solved for four different discrete values of n, each value with its blocking mechanism, as shown in Figure 1 and Equations 1-4.

$$\frac{d^2t}{dV^2} = k\left(\frac{dt}{dV}\right)^n \qquad \text{Eq. 1}$$

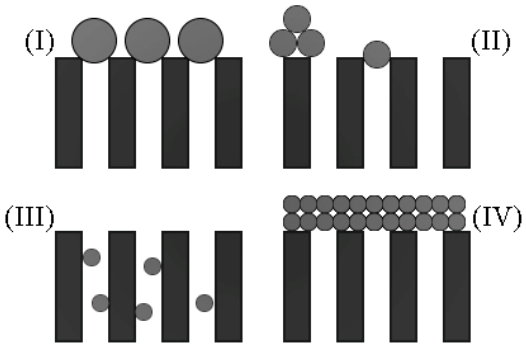

Figure 1. Blocking mechanisms by Hermia (1982): (I) complete blocking; (II) intermediate blocking; (III) standard blocking; (IV) cake formation.

Complete blocking (CB) ($n = 2$)	$\ln j = \ln j_0 - k \cdot t$	Eq. 2
Intermediate blocking (IB) ($n = 1$)	$1/j = (1/j_0) - k \cdot t$	Eq. 3
Standard blocking (SB) ($n = 3/2$)	$1/\sqrt{j} = (1/\sqrt{j_0}) - k \cdot t$	Eq. 4
Cake formation (CF)($n = 0$)	$1/j^2 = (1/j_0^2) - k \cdot t$	Eq. 5

Where t is the time measured from the beginning of the filtration experiment, j is the permeate flux at time t, j_0 is the permeate flux at time $t = 0$ and k is a real constant determined experimentally. The simplicity and effectiveness of this model made their way into the application of membrane filtration, such as the ultrafiltration of polyethylene glycol, in which all pore-blocking mechanisms performed similarly, with complete blocking (CB) having R^2 between 0.621 and 0.913, intermediate blocking (IB) having R^2 between 0.638 and 0.923, standard blocking (SB) having R^2 between 0.635 and 0.918, and cake formation (CF) having R^2 between 0.639 and 0.947 for crossflow velocities (CFVs) of 1-3 m/s and transmembrane pressures (TMPs) of 0.1-0.4 MPa [2].

Applications in cross-flow ultrafiltration of effluent from a railway workshop yielded more consistent results for all four blocking mechanisms, with correlation coefficients between 0.75 and 0.88 for CB, between 0.88 and 0.92 for IB, between 0.83 and 0.91 for SB, and between 0.97 and 0.98 for CF for TMPs of 21, 35, and 48 kPa [3]. Similar representative behavior is also found in the nanofiltration of polycyclic aromatic hydrocarbons in membranes NF270 and NF10, with CB having R^2 of 0.863 and 0.988, IB having 0.936 and 0.988, SB having 0.947 and 0.991, and CF having 0.908 and 0.957, respectively [4].

Although the Hermia model can perform well with the original four values of n, there are applications where the permeate flux is discontinuous, such as the removal of glycerol from biodiesel at TMPs of 1 to 3 bar [5,6], or changes in pH in high-pressure wastewater nanofiltration [7], in which these values of n cannot accommodate experimental data. Therefore, this model has been modified to better accommodate experimental results by increasing its complexity, either by keeping the same blocking mechanisms but changing the equations, such as in glycerin-water solutions, where simple changes in the original equations yielded R^2 between 0.6951 and 0.8611 for complete blocking, between 0.8489 and 0.9622 for intermediate blocking, between 0.8189 and 0.9315 for standard blocking, and between 0.7896 and 0.9468 for cake formation [8].

Other modifications can be applied by using the concept of flow resistance, as in the microfiltration of oil-in-water emulsions, in which a modified Hermia model is used in conjunction with the first and second derivatives of the flow resistance. This setup yields a system of ODEs that results in the behavior of flux, $j(t)$ [9]. Still, both these modifications use the original Hermia model as the base. Similar approaches have been used to model fouling in micro- and ultrafiltration

membranes for treating limed and partially clarified sugar cane juice, such as the use of cake filtration (CFM) and combinations of external and progressive internal fouling models (CEPIFM). In the case of treating limed and partially clarified sugar cane juice, these models can perform well, with R^2 between 0.9939 and 0.9992 for CFM, and 0.9718 and 0.9883 for CEPIFM [10].

Although the use of more complex models, such as CFM and CEPIFM does indeed improve the predictability of $j(t)$ and the accumulated volume of permeate, it comes at the cost of simplicity. Therefore, this paper aims to mathematically prove a more general version of the Hermia model, as well as make fitting experimental data simpler and more effective without having to use complicated equations. We have also aimed to use the extended Hermia model in different examples and compare its performance to the original four pore-blocking mechanisms (Eq. 1-4).

2. Materials and Methods

2.1. Control Volume and Model Setup

Inside of a module (Figure 2) of constant cross-sectional area A with a constant mass flux N_0, some mass from this flux will be retained by the membrane making it harder for more mass to pass through the membrane as permeate. Consequently, over time, the exit mass flux $N(t)$ should decrease. In this model, the mass accumulated is modeled by a porous solid with a constant base area A and thickness $\delta(t)$. After an infinitesimal time Δt, the mass accumulated makes δ to increase. Therefore, it is possible to take this solid as the control volume (CV) and apply conservation laws to it.

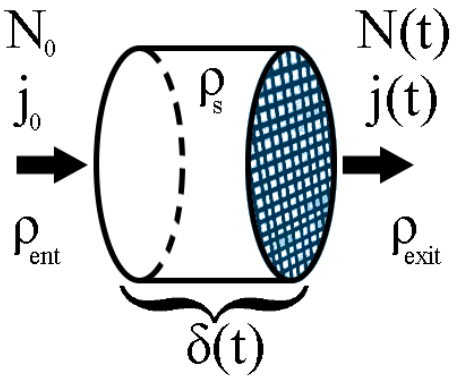

Figure 2. The control volume is solid with a constant cross-sectional area A and density ρ_s, such that the entering stream of fluid has a constant mass flux N_0, a constant permeate flux j_0 and density ρ_{ent}. The exiting stream of fluid has a mass flux $N(t)$, a permeate flux $j(t)$, and a density ρ_{exit}. The thickness $\delta(t)$ increases over time as more mass is accumulated on the membrane (shown as a shaded section).

2.2. Continuity Equation

The continuity equation (Eq. 5), also known as the general conservation of mass equation [13] or as the mass balance equation [11,12], is the mathematical formula that keeps track of how much mass is inside of a given control volume. It does so by computing how much the control volume itself changes over time, which is given by the volume integral, and by calculating how much mass leaves or enters the CV, which is given by the surface integral.

$$\frac{\partial}{\partial t}\iiint_{CV} \rho d\forall + \iint_{CS} \rho(\vec{j}\cdot\vec{n})dA = 0 \qquad \text{Eq. 6}$$

Where ρ is the density function, $d\forall$ is the volume differential of the CV, $\vec{j}$ is the velocity vector, $\vec{n}$ is the vector perpendicular to the surface of the CV and dA is the differential surface area of the CV.

2.3. Hermia's Experimental Model

The differential equation (Eq. 1 or Eq. 7) is an experimental result obtained by Hermia [1], which correlates the second derivative of time (t) concerning the accumulated volume (V) with the first derivative of t with respect to V.

$$\frac{d^2t}{dV^2} = k\left(\frac{dt}{dV}\right)^n \quad \text{Eq. 7}$$

Here, the coefficients k and n are two real numbers that can be changed to better adjust the model for different situations. As discussed in Section 1, the model was originally solved for $n = 2, 1{,}3/2, 0$. These solutions resulted in Eq. 2, Eq. 3, Eq. 4, and Eq. 5, respectively.

2.4. Derivatives of Inverse Functions

For a given function $y(x)$ and its inverse function given by $x(y)$, the relationship between dy/dx and dx/dy, if $y(a) = b$, is given by [13]:

$$\left(\frac{dy}{dx}\right)_{x=a} \cdot \left(\frac{dx}{dy}\right)_{y=b} = 1 \quad \text{Eq. 8}$$

As for the second derivatives of these functions:

$$\left(\frac{d^2y}{dx^2}\right)_{x=a} = -\left(\frac{d^2x}{dy^2}\right)_{y=b} \cdot \left[\left(\frac{dy}{dx}\right)_{x=a}\right]^3 \quad \text{Eq. 9}$$

For the sake of brevity, the proof does not use the full subscript (e.g., $x = a$). It only discloses the direct values of the independent variables. As an example, $(dy/dx)_{x=a}$ would be written as $(dy/dx)_a$

2.5. Flux Definition

One of the definitions of mass flux of a given stream i is given by the product between its mass concentration/total density (ρ_i) and its velocity (j_i) [11,12], as stated in Eq. 10.

$$N_i = \rho_i j_i \quad \text{Eq. 10}$$

2.6. Accumulated Volume and Flux

As presented in Eq. 11, the accumulated volume $V(t)$ for a mass flux $N(t)$ can be calculated by integrating $N(t)$ from t = 0 to t = t, which will give the total mass per unit of cross-sectional area. Therefore, multiplying by the area and dividing by its density will yield the accumulated volume, $V(t)$.

$$V(t) = \frac{A}{\rho_{exit}} \int_0^t N(t)dt \quad \text{Eq. 11}$$

2.7. Integral Properties

A reduced form of the Leibnitz formula with constant integration limits a and b for a given function $y(x)$ yields Eq. 12 [14].

$$\int_a^b \left[\frac{dy(x)}{dx}\right] dx = y(b) - y(a) \quad \text{Eq. 12}$$

3. Results

Taking into account Eq. 1-4, it is possible to observe that, apart from $n \neq 2$, $j(t)$ seems to follow a pattern, such that, if the reduced permeate flux (j/j_0) is isolated in Eq 2-4:

Intermediate blocking ($n = 1$)	$j/j_0 = 1/(1 - k \cdot t \cdot j_0)$	Eq. 13
Standard blocking ($n = 3/2$)	$(j/j_0)^{1/2} = 1/(1 - k \cdot t \cdot \sqrt{j_0})$	Eq. 14
Cake formation ($n = 0$)	$(j/j_0)^2 = 1/(1 - k \cdot t \cdot j_0^2)$	Eq. 15

Since k is a real number and j_0 is a constant, Eq. 12-14 can be rewritten as one equation (Eq. 16) with a variable exponent P, where $P \neq 0$.

$$\left[\frac{j(t)}{j_0}\right]^P = \frac{1}{(1 + k \cdot t)} \qquad \text{Eq. 16}$$

In this context, the pore-blocking mechanisms would be given by different values of P, such that $P = 1$ is intermediate blocking, $P = 1/2$ is standard blocking, and $P = 2$ is cake formation. Furthermore, it is possible to establish a relationship between P and n, such that $P = 2 - n$. For $n = 2$ (or $P = 0$), the reduced permeate flux is simply given by Eq. 17.

$$\frac{j(t)}{j_0} = exp(-k \cdot t) \qquad \text{Eq. 17}$$

We have wondered if other values of P can be used in Eq. 16 to better represent experimental data, expanding the original model into a sort of extended Hermia model (EHM). Therefore, we have performed the model fitting for all four original pore-blocking mechanisms and the EHM in Examples 1, 2, 3, 4, 5, and 6 to have a better understanding of how these mechanisms change in different contexts. In these Examples, we have obtained consistently better performance than the four original pore-blocking mechanisms. Thus, to justify the use of the EHM, we have also used Eq. 5-11 and proven Theorems 1, 2, and 3. Their proofs can be found in Appendices A, B, and C, respectively.

Theorem 1. *The original Hermia model can be extended to accommodate new values of P. If both the fluid and the permeate have similar densities, then the flux $j(t)$ can be expressed by Eq. 18 for any $P \neq 0$. If $P = 0$, then then the flux $j(t)$ can be expressed by Eq. 19.*

$$\left[\frac{j(t)}{j_0}\right]^P \approx \frac{1}{(1 + k \cdot t)} \qquad \text{Eq. 18}$$

$$j(t) \approx j_0\, exp(-k \cdot t) \qquad \text{Eq. 19}$$

A measure of how fast $\boldsymbol{j(t)}$ declines over time can be given by applying both Eq. 18 and Eq. 19 and calculating the amount of time needed for the reduced permeate flux to drop by half $\left(\frac{j(t)}{j_0} = 0.5\right)$. We will refer to this quantity as the EHM half-life (Eq. 20).

$$t_{1/2} = \begin{cases} \dfrac{\left(\frac{1}{0.5^P} - 1\right)}{k}, & P \neq 0 \\ -\dfrac{\ln 0.5}{k}, & P = 0 \end{cases} \qquad \text{Eq. 20}$$

Therefore, for as given $\boldsymbol{P}$, there is a p^{th}-degree blocking mechanism. This means intermediate blocking is a 1^{st}-degree blocking mechanism, that cake formation is a 2^{nd}-degree blocking mechanism, that, and so on.

Theorem 2. *If the EHM has been correctly fitted to experimental data and represents the dataset well (such as with a low RMSE or with a high R^2), then the fouling layer's thickness can also be fitted to the profile given by Eq. 21.*

$$\delta(t) = \begin{cases} (k_{15} + k_{16}t)^{-\frac{1}{P}+1} - k_{15}^{-\frac{1}{P}+1} + k_{12}t, & P \neq 0 \\ k_{19}[\exp(-k_9 t) - 1] + k_{20}t, & P = 0 \end{cases} \quad \text{Eq. 21}$$

Theorem 3. *If the EHM has been correctly fitted to experimental data and represents the dataset well (such as with a low RMSE or with a high R^2), then the accumulated permeate volume can be calculated using Eq. 22.*

$$V(t) = \begin{cases} \frac{j_0 \cdot A}{k\left(1 - \frac{1}{P}\right)}\left([1 + k \cdot t]^{\left(1-\frac{1}{P}\right)} - 1\right), & P \neq 0 \\ \frac{j_0 \cdot A}{k}[1 - exp(-k \cdot t)], & P = 0 \end{cases} \quad \text{Eq. 22}$$

Example 1. *Model fitting for ultrafiltration membrane used in different wastewater pretreatment conditions*

In a paper by Jung and Son, a pretreatment of organic matter coagulation and MIEX® was evaluated on a bench-scale filtration apparatus. This work investigated many different pretreatment conditions and their impact on micro- and ultrafiltration in hydrophilic (HPI) and hydrophobic (HPO) membranes. While keeping TMP at 1 bar for microfiltration and 2 bar for ultrafiltration, both coagulant and MIEX® were added to the wastewater and the filtration was carried out [15].

In this example, we have isolated the data obtained from ultrafiltration for both HPI and HPO membranes with and without the addition of coagulant 140 mg/L and MIEX® 12 mL/L. We have performed the model fitting for all four pore-blocking mechanisms and the extended Hermia model by minimizing the root mean square error (RMSE). These regressions can be found in Appendix D (Figure D 1-Figure D 8), Table 1, and Table 2.

Table 1. EHM parameters for the regressions obtained in Example 1.

Case	Filtration conditions	*P*	*K* (h^{-1})	EHM half-life (h)
1	HPI only	2.76	10.22	0.57
2	Coag. 140 mg/L+HPI	4.43	9.56	2.15
3	MIEX 12 mL/L	2.88	9.33	0.68
4	MIEX 12 mL/L+Coag. 40 mg/L+HPI	3.08	2.41	3.11
5	HPO only	2.23	99.20	0.04
6	Coag. 140 mg/L+HPO	3.04	24.82	0.29
7	MIEX 12 mL/L+HPO	1.85	25.94	0.10
8	MIEX 12 mL/L+Coag. 40 mg/L+HPO	2.97	17.49	0.39

Table 2. RMSE results obtained in Example 1.

Case	Filtration conditions	CB	IB	SB	CF	EHM
1	HPI only	0.0795	0.0449	0.0612	0.0178	0.0048
2	Coag. 140mg/L+HPI	0.0593	0.0429	0.0508	0.0287	0.0065
3	MIEX 12mL/L	0.0725	0.0423	0.0566	0.0184	0.0054
4	MIEX 12mL/L+Coag. 40mg/L+HPI	0.025	0.0164	0.0206	0.0090	0.0046
5	HPO only	0.13320	0.0598	0.0936	0.0134	0.0101
6	Coag. 140mg/L+HPO	0.1104	0.0634	0.0851	0.0287	0.0078

Preprints (www.preprints.org) | NOT PEER-REVIEWED | Posted: 5 January 2023 doi:10.20944/preprints202206.0187.v2

Peer-reviewed version available at Membranes 2023, 13, 290; doi:10.3390/membranes13030290

7	**MIEX 12mL/L+HPO**	0.1161	0.0429	0.0753	0.0099	0.0077
8	**MIEX 12mL/L+Coag. 40mg/L+HPO**	0.0962	0.0555	0.0744	0.025	0.0085

Based on the regressions obtained, we have noticed that the extended Hermia model has a better performance when comparing the four blocking mechanisms (RMSE≤0.01), followed by the cake formation mechanism. Although the EHM provides better estimates for flux, cases 1, 2, 3, 4, 5, 6, and 8 have $P > 2$, which can be physically interpreted as a new blocking mechanism.

For cases 5 and 7 we have obtained values of P that are relatively close to the cake formation mechanism which implies that this type of blocking can happen to a certain degree. As an example, case 7 shows that $2 \geq P \geq 1$, therefore, we can physically interpret this as a mixture of both cake formation and intermediate blocking. As for cases 3, 5, and 8, the same principle can be applied, therefore, these cases indicate a mixture of cake formation and a 3rd-degree blocking mechanism. Comparing both HPI and HPO membranes with no additions, the EHM predicts that the HPI membrane has a half-life of 0.57 h, meanwhile the HPO membrane has a half-life of only 0.04 h. This indicates that for this example fouling greatly affects HPO membranes when compared to HPI membranes. We have also noticed that the addition of coagulant and MIEX® increased the half-life for both HPI and HPO membranes.

This effect can be explained by the changes in the pore-blocking mechanism since the values of P change with the addition of coagulant and MIEX®. With no additives the mechanism tends to cake formation ($P = 2.76$ for HPI and $P = 2.23$ for HPO) but the addition of coagulant shifts to a 4th-degree blocking mechanism for HPI and a 3rd-degree blocking mechanism for HPO ($P = 4.43$ for HPI and $P = 3.04$ for HPO). The addition of MIEX® changes the blocking mechanisms slightly ($P = 2.88$ for HPI and $P = 1.85$ for HPO). As a result, we can infer that the most significant change to the pretreatment is the addition of the coagulant, which increases EMH half-life considerably by changing the pore-blocking mechanism. Therefore, given the results presented in **Table 1**, both additives used with the HPI membrane give a considerable increase in EMH half-life, which indicates that this is a better solution for fouling reduction in Example 1.

Example 2. *Model fitting for microfiltration with ceramic membranes used in corn syrup clarification*

In a paper by Almandoz and coauthors, 3 different ceramic membranes (CM08, CM05, and CM01) were evaluated at different CFVs and TMPs considering the removal of undesired oil, protein, and other non-starch components. The main difference between the ceramic membranes is their structure, mainly represented by properties such as mean pore radius obtained through volume mercury penetration (r_p), hydraulic permeability (L_h) and porosity (ε). Microfiltration was carried out at 0.5 m/s and 50 kPa for all three membranes and CM05 was chosen for the following experiments due to better performance such as lower turbidity, lower concentrations of insoluble residues, and total proteins [16]. We have recovered the data obtained throughout the experiments with CM08, CM05, and CM01 and performed the model fitting for all four pore-blocking mechanisms and the EHM. We have also isolated the data for different TMP conditions for microfiltration with CM05. These results can be found in Appendix D (Figure D 9-Figure D 14), Table 3, Table 4, Table 5, and Table 6.

Table 3. EHM parameters for the regressions obtained in Example 2 for CM08, CM05, and CM01.

Membrane	P	K (h^{-1})	EHM half-life (h)
CM08	1.49	6.67	0.27
CM05	1.25	2.48	0.56
CM01	2.67	11.19	0.48

Table 4. RMSE results obtained in Example 2 for CM08, CM05, and CM01.

Membrane	CB	IB	SB	CF	EHM
CM08	**0.1076**	**0.0402**	**0.0694**	**0.0381**	**0.0285**

CM05	**0.0811**	**0.0258**	**0.0473**	**0.0382**	**0.0225**
CM01	**0.151**	**0.0814**	**0.1119**	**0.0427**	**0.0351**

According to Table 3 and Table 4, the EHM has performed better than the four classic pore-blocking mechanisms (RMSE≤0.035), followed by cake formation (RMSE≤0.042). We have also noticed that the pore-blocking mechanism varies from membrane to membrane in the present example. Both CM08 and CM05 have a 1st-degree pore-blocking mechanism (between intermediate blocking and cake formation), while CM01 has a 2nd-degree blocking (between cake formation and a possible new type of pore-blocking). Meanwhile, the EMH half-life calculated for CM05 reveals that fouling doesn't affect this membrane as much as it does CM08 and CM01, therefore this membrane has been chosen by Almandoz and coauthors for later tests [16]. We have consolidated the data from these later tests and performed the same analysis. The regression results are presented in Table 5 and Table 6.

Table 5. EHM parameters for the regressions obtained in Example 2 for CM05 at different TMPs.

TMP	P	K (h^{-1})	EHM half-life (h)
103.42kPa	1.21	3.08	0.43
51.71kPa	1.61	4.48	0.46
37.9kPa	1.69	5.41	0.41

Table 6. RMSE results obtained in Example 2 for CM05 at different TMPs.

TMP	CB	IB	SB	CF	EHM
103.42kPa	0.0912	0.0318	0.0545	0.0485	0.0293
51.71kPa	0.1090	0.0411	0.0698	0.0306	0.0257
37.9kPa	0.1047	0.0388	0.0676	0.0223	0.0184

Taking into consideration Table 5 and Table 6, the best-performing models are EHM, cake formation, and intermediate blocking. At times intermediate blocking performs better than cake formation, yet the EHM still performs better than both. It is also interesting to point out that Figures have EHM with $2 \geq P \geq 1$, indicating that a mixed blocking mechanism between intermediate blocking and cake formation can happen simultaneously. In this case, it seems that an increase in TMP causes a slight shift in the most prevalent blocking mechanism from cake formation to intermediate blocking since P goes from 1.69 to 1.21. We have noticed that the middle ground between cake formation and intermediate blocking slightly increases the EHM half-life, which is the desired outcome when optimizing the filtration conditions.

Example 3. *Model fitting for cross-flow hollow fiber ultrafiltration of oily effluent from a railway workshop*

In a paper by Kurada and Tanmay [17], oily effluent containing dust, grease, and oil has been treated by a sand bed followed by a cross-flow ultrafiltration hollow fiber membrane. Their experimental work involved changing both TMP (21-104 kPa) and CFR (14-40 L/min) and evaluating the aftermath, such as flux reduction and cake layer thickness. We have extracted the data obtained by Kurada and Tanmay and applied the same techniques presented in Examples 1 and 2. The regression results and EHM parameters can be found in Appendix D (Figure D 15-Figure D 23), Table 7, and Table 8.

Table 7. EHM parameters for the regressions obtained in Example 3.

Filtration conditions	P	K (min^{-1})	EHM half-life (min)
CFR 14 L/min 21 kPa	1.56	0.38	5.10
CFR 14 L/min 35kPa	1.49	0.37	4.85
CFR 14 L/min 104kPa	1.47	0.37	4.77
CFR 28L/min 21kPa	1.43	0.37	4.62

Preprints (www.preprints.org) | NOT PEER-REVIEWED | Posted: 5 January 2023 doi:10.20944/preprints202206.0187.v2

Peer-reviewed version available at Membranes 2023, 13, 290; doi:10.3390/membranes13030290

CFR 28L/min 35kPa	1.50	0.39	4.72
CFR 28L/min 104kPa	1.49	0.39	4.66
CFR 40L/min 21kPa	1.51	0.40	4.68
CFR 40L/min 35kPa	1.50	0.39	4.66
CFR 40L/min 104kPa	1.58	0.45	4.42

Table 8. RMSE results obtained in Example 3.

Filtration conditions	CB	IB	SB	CF	EHM
CFR 14L/min 21 kPa	0.1266	0.0572	0.0892	0.0492	0.0424
CFR 14L/min 35kPa	0.1183	0.0505	0.0821	0.0476	0.0377
CFR 14L/min 104kPa	0.1164	0.0494	0.0806	0.0486	0.0377
CFR 28L/min 21kPa	0.1129	0.0475	0.0779	0.0499	0.0373
CFR 28L/min 35kPa	0.1177	0.0500	0.0818	0.0469	0.0369
CFR 28L/min 104kPa	0.1171	0.0499	0.0814	0.0475	0.0372
CFR 40L/min 21kPa	0.1197	0.0513	0.0832	0.0467	0.0375
CFR 40L/min 35kPa	0.1168	0.0488	0.0808	0.0455	0.0353
CFR 40L/min 104kPa	0.1168	0.0454	0.0800	0.0345	0.0256

Based on the regressions presented in Table 7 and Table 8, we have observed a very similar behavior to Example 2, in which the best performance was credited to the EHM (RMSE≤0.042). cake formation and intermediate blocking have also performed well (RMSE≤0.049 and ≤0.057 respectively). In Example 2 we have pointed out that an increase in TMP changes the most prevalent pore-blocking mechanism from cake formation into intermediate blocking because P had its value decreased. The same effect is also present here but only for a CFR of 14 L/min. For CFRs of 28 and 40 L/min, is seems that P behaves differently, increasing or decreasing with TMP. Changes in CFR while maintaining TMP constant also seem to have the same effect. Therefore, for the present Example, it seems that significant changes in TMP and CFR do not change the pore-blocking mechanism considerably. We have also noticed that decreasing both TMP and CFR leads to an increase in EHM half-life since, in this case, P tends to cake formation and lower values of TMP and CFR prevent the cake layer thickness from increasing as rapidly.

As a consequence, rather than looking at which experimental conditions lead to the most advantageous pore-blocking mechanism, we have to analyze which conditions result in higher values of j_0 and how it affects the accumulated permeate volume given in Eq. 22 (Figure 3).

Preprints (www.preprints.org) | NOT PEER-REVIEWED | Posted: 5 January 2023 doi:10.20944/preprints202206.0187.v2

Peer-reviewed version available at Membranes 2023, 13, 290; doi:10.3390/membranes13030290

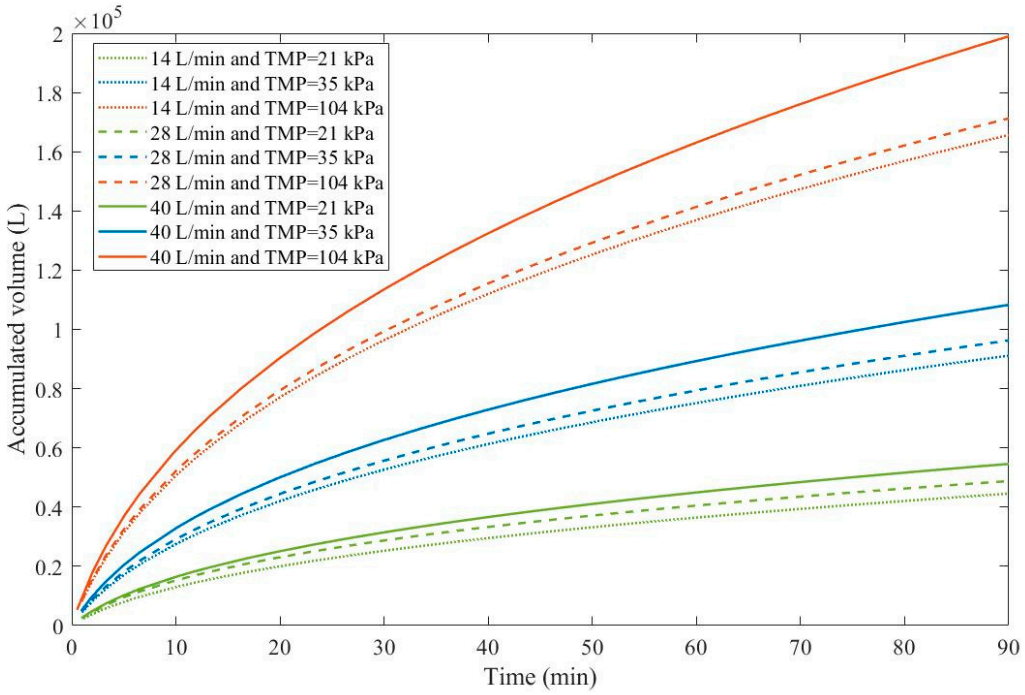

Figure 3. The accumulated volume calculated through the EHM for oily effluent ultrafiltration with CFR of 14-40L/min and 21-104kPa assuming $A = 1.00\ m^2$

We have color-coded Figure 3 for a better understanding. TMP is represented in different colors, green for 21 kPa, blue for 35 kPa, and red for 104 kPa. Full lines represent 40 L/min, discontinued lines represent 28 L/min and dotted lines represent 14 L/min. Through Figure 3, we have noticed that an increase in TMP causes a general increase in the accumulated volume for all CFRs. For all TMPs we have observed an increase in CFR also causes an increase in the accumulated volume. Therefore, in Example 3, higher TMPs and CFRs are advantageous. It is important to point out that this effect is only possible because changes in both TMP and CFR do not change the blocking mechanism greatly, as shown in Table 7. For instance, in Example 4 we demonstrate that an increase in crossflow velocity can either increase or decrease the accumulated volume depending on the blocking mechanism.

Example 4. *Model fitting for ultrafiltration of alkali/surfactant/polymer flooding wastewater*

In an experimental work by Ren et al., ultrafiltration was used to treat Alkali/surfactant/polymer (ASP) flooding wastewater, a commonly produced effluent in enhanced oil extraction processes that needs to be properly treated before reuse due to the potential threat of formation damage. In this study, the operating parameters were modified to research their effects on membrane fouling, which aimed to optimize the filtration conditions to minimize the effect of flux reduction. These parameters included TMP (2.12-2.79 bar) and CFV (0.75-3.00 m/s), with the ideal conditions being a TMP of 2.12 bar and CFV of 3.00 m/s [18].

We have recovered the flux data obtained by Ren et al. and performed the model fitting for all four classic pore-blocking mechanisms and the EHM. These results are presented in Appendix D (Figure D 24-Figure D 29), Table 9, Table 10, Table 11, and Table 12.

Table 9. EHM parameters for the regressions obtained in Example 4 at 2.5 m/s and different TMPs.

Filtration conditions	P	K (h^{-1})	EHM half-life (h^{-1})
2.12 bar	9.67	5.54	146.33
2.79 bar	4.38	3.19	6.20

Table 10. RMSE results obtained in Example 4 at 2.5 m/s and different TMPs.

Filtration conditions	CB	IB	SB	CF	EHM
2.12 bar	0.0768	0.0653	0.0709	0.0548	0.00930
2.79 bar	0.1028	0.0715	0.0863	0.0466	0.0151

According to Table 9 and Table 10, across all the model fittings, the EHM presents the best data fit (RMSE≤0.015), as the other pore-blocking mechanisms, do not seem to fit the data accurately. We have noticed that an increase in TMP causes a decrease in the value of P changing the pore blocking mechanism from a 9th-degree to a 4th-degree. The present example was included to demonstrate that even though the EHM fits the data well, it is important to exercise caution when doing so. The EHM half-life, when calculated using Eq. 20, yields results that are not physically accurate. Since the data recovered from Ren et al. does not include $\frac{j}{j_0} > 0.14$ in Figure D 24-Figure D 29, the values obtained for P and K do not represent values $\frac{j}{j_0} > 0.14$. Therefore, the use of Eq. 20 extrapolates the model for points that were not included in the regression, which results in EHM half-life values that are non-representative. The same regressions have been performed on the experimental tests at 2.20 bar with varying CFV (0.75-3.00 m/s) (Table 11 and Table 12).

Table 11. EHM parameters for the regressions obtained in Example 4 for different cross-flow velocities.

Filtration conditions	P	K (h^{-1})	EHM half-life (h)
0.75 m/s	7.84	81.12	2.82
1.50 m/s	5.96	22.37	2.73
2.25 m/s	8.34	36.02	8.96
3.00 m/s	9.05	33.38	15.84

Table 12. RMSE results obtained in Example 4 for different cross-flow velocities.

Filtration conditions	CB	IB	SB	CF	EHM
0.75 m/s	0.1796	0.1419	0.1599	0.1108	0.0369
1.50 m/s	0.1553	0.1161	0.1346	0.0850	0.0277
2.25 m/s	0.1479	0.1192	0.1331	0.0947	0.0242
3.00 m/s	0.1341	0.1103	0.1218	0.0897	0.0215

Taking into account Table 11 and Table 12, we have observed that the EHM had a better performance (RMSE≤0.037) when compared to the four original pore-blocking mechanisms. For the present example, it seems that changes in CFV affect P greatly, changing between 5th-degree and 9th-degree mechanisms. Once again, the EHM half-life is not physically representative because it is extrapolating the model, such as in Table 9, therefore if this happens in the following Examples (Example 5 and Example 6), the EHM half-life will be referred to as non-applicable (N/A). One alternative to better rank the filtration conditions to optimize the process is to use Eq. 22. By calculating the accumulated volume of permeate, it is possible to obtain a function of P and K, making it possible to rank the filtration conditions through accumulated volume maximization. Figure 4 presents the accumulated volume calculated using Eq. 22 assuming a $j_0 = 100\ L/m^2h$ and $A = 1.567\ m^2$ for all CFVs.

Preprints (www.preprints.org) | NOT PEER-REVIEWED | Posted: 5 January 2023 doi:10.20944/preprints202206.0187.v2

Peer-reviewed version available at Membranes 2023, 13, 290; doi:10.3390/membranes13030290

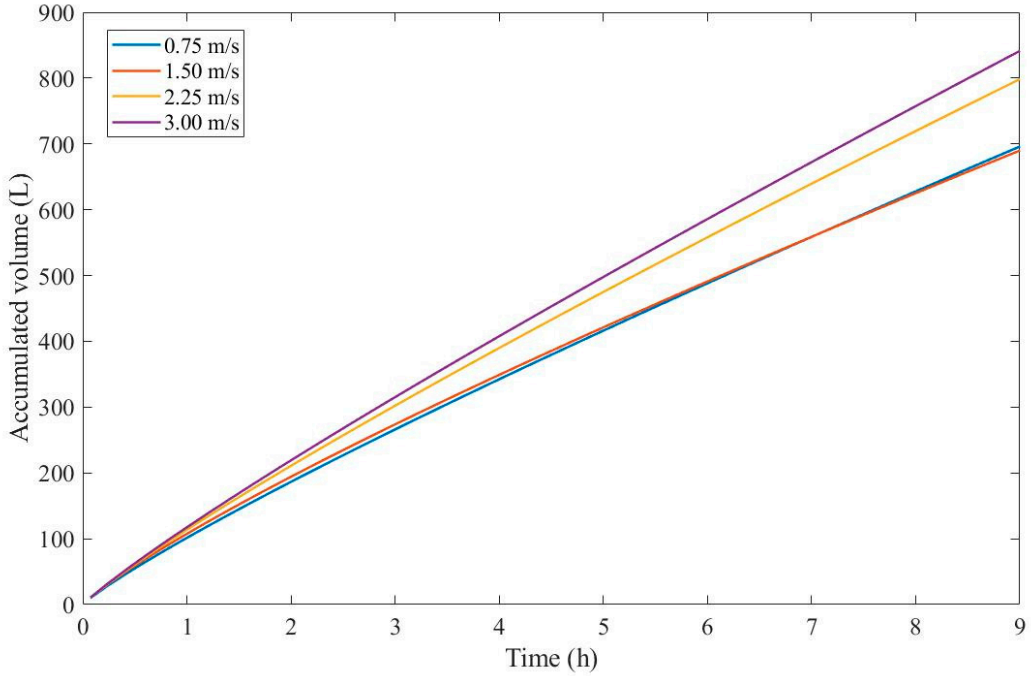

Figure 4. The accumulated volume calculated through the EHM for ultrafiltration of flooding wastewater at 2.20bar and cross-flow velocities of 0.75-3.00 m/s assuming a $j_0 = 100\ L/m^2h$ and $A = 1.567\ m^2$

Through Figure 4, we have calculated that an accumulated volume for a CFV of 3.00 m/s yields better results, therefore a 9th-degree pore-blocking mechanism is favorable in this context. Due to the non-linear nature of Eq. 22, a higher CFV will not always provide higher values for the accumulated volume, as shown in Figure 4 for CFVs of 0.75 and 1.50 m/s. At one point both of their curves meet, which means that, at times, fouling will affect the membrane to such a degree that lower CFVs would yield a higher permeate production.

Example 5. *Model fitting for ultrafiltration of bovine serum albumin solutions*

Aiming to decrease the effects of fouling in iron oxide ultrafiltration membranes, Storms and collaborators coated these ceramic membranes with poly(sulfobetaine methacrylate) (polySBMA), a superhydrophilic zwitterionic polymer and investigated whether this modification was helpful towards flux reduction. Albumin solutions were filtered at a TMP of 103.421 kPa in three fouling stages for both uncoated and coated membranes, such that washings were performed between stages [19].

We have recovered the experimental data obtained for the three fouling stages for both uncoated and coated membranes. The same model fitting performed in Examples 1-Example 4 was also applied to the present example. The regressions obtained are presented in Appendix D (Figure D 30-Figure D 35), Table 13, and Table 14.

Table 13. EHM parameters for the regressions obtained in Example 5.

Filtration conditions	P	K (h^{-1})	EHM half-life (h)
First fouling stage (Uncoated membrane)	1.33	3.28	0.46
Second fouling stage (Uncoated membrane)	1.38	2.47	0.65
Third fouling stage (Uncoated membrane)	4.03	1.19	N/A
First fouling stage (Coated membrane)	1.42	2.22	0.75
Second fouling stage (Coated membrane)	2.18	4.67	0.76
Third fouling stage (Coated membrane)	2.67	1.872	N/A

Table 14. RMSE results obtained in Example 5.

Filtration conditions	CB	IB	SB	CF	EHM
First fouling stage (Uncoated membrane)	0.1122	0.04690	0.07190	0.05480	0.04190
Second fouling stage (Uncoated membrane)	0.1263	0.06240	0.08800	0.06690	0.05630
Third fouling stage (Uncoated membrane)	0.08860	0.06430	0.07590	0.04510	0.02730
First fouling stage (Coated membrane)	0.09500	0.04030	0.06220	0.04270	0.03400
Second fouling stage (Coated membrane)	0.1616	0.09510	0.1235	0.06880	0.06820
Third fouling stage (Coated membrane)	0.08090	0.05350	0.06610	0.03710	0.03390

By the results presented in Table 13 and Table 14, we have demonstrated that the EHM performs better than the original four pore-blocking mechanisms since it has an RMSE≤0.068. According to the values obtained for P, the addition of polybag changes the pore-blocking mechanism for the first fouling stage, which starts with a prevalent mechanism of intermediate blocking and changes slightly to cake formation since P goes from 1.33 to 1.42. This change is further supported by the second fouling stage, in which $P = 1.38$ for the uncoated membrane and 2.18 for the coated membrane. The third fouling stage shows that the uncoated membrane has a big shift in the pore-blocking mechanism going from a mainly intermediate blocking (1st-degree) to a 4th-degree. In contrast, the third fouling stage for the coated membrane stays mainly a cake formation mechanism (2nd-degree).

We have also observed an increase in EHM half-life in the first and second fouling stages, which indicated that the addition of polySBMA does mitigate fouling to a certain degree. It is also interesting to point out that the polySBMA coating seems to cause a cake formation mechanism, which, in this case, is advantageous since it increases the EHM half-life and the amount of permeate obtained per filtration batch.

Example 6. *Model fitting for ultrafiltration of nanoparticles from polishing wastewater*

In a series of ultrafiltration experiments at a laboratory scale conducted by Ohanessian et al., chemical mechanical polishing wastewater filtration was carried out to optimize and validate fouling models. Two types of experiments have been performed: dead-end filtration at a TMP of 0.4 bar and crossflow filtration at a TMP of 0.3 bar. Different concentrations were evaluated for both, 97, 251, and 657 mgNPs/L (milligrams of nanoparticles per liter) for dead-end filtration and 332, 572, and 2600 mgNPs/L for crossflow filtration [20].

We have recovered the data from the dead-end filtration experiments and performed the model fitting for all original pore-blocking mechanisms, as well as the EHM. The regression results are presented in Appendix D (Figure D 36-Figure D 38), Table 15, and Table 16.

Table 15. EHM parameters for the regressions obtained in Example 6 at 0.4 bar and different nanoparticle concentrations.

Filtration conditions	P	K (s^{-1})	EHM half-life (s)
97 mgNPs/L	3.60	0.026	426.52
251 mgNPs/L	2.06	0.014	229.94
657 mgNPs/L	2.80	0.187	31.91

Table 16. RMSE results obtained in Example 6 at 0.4 bar and different nanoparticle concentrations.

Filtration conditions	CB	IB	SB	CF	EHM
97 mgNPs/L	0.1271	0.0806	0.1004	0.0552	0.0425
251 mgNPs/L	0.1276	0.0609	0.0908	0.0294	0.0292
657 mgNPs/L	0.1480	0.0822	0.1124	0.0398	0.0288

According to Table 15 and Table 16, throughout the experiment, the EHM has consistently performed better than the original pore-blocking mechanisms (RMSE≤0.042) followed closely by the cake formation mechanism (RMSE≤0.055). We have also noticed that an increase in the concentration of nanoparticles non-linearly changes the pore-blocking mechanism, starting at a 3rd-degree and moving to a mostly cake formation mechanism (2nd-degree). In contrast, a further increase in nanoparticle concentration does the opposite, changing from mostly cake formation to a mixed pore-blocking mechanism of cake formation and 3rd-degree blocking.

Taking into account the EHM half-life, it seems that an increase in nanoparticle concentration is directly correlated with a decrease in half-life, which indicates that fouling has a bigger effect at higher concentrations. It is important to point out that the flux data presented in Figure D 36-Figure D 38 have different values of j_0 for each concentration, therefore, to better classify which pore-blocking mechanism is the most advantageous in Example 6, we have used Eq. 22 and the regression results to calculate the accumulated permeate volume (Figure 5) assuming $A = 1\ m^2$.

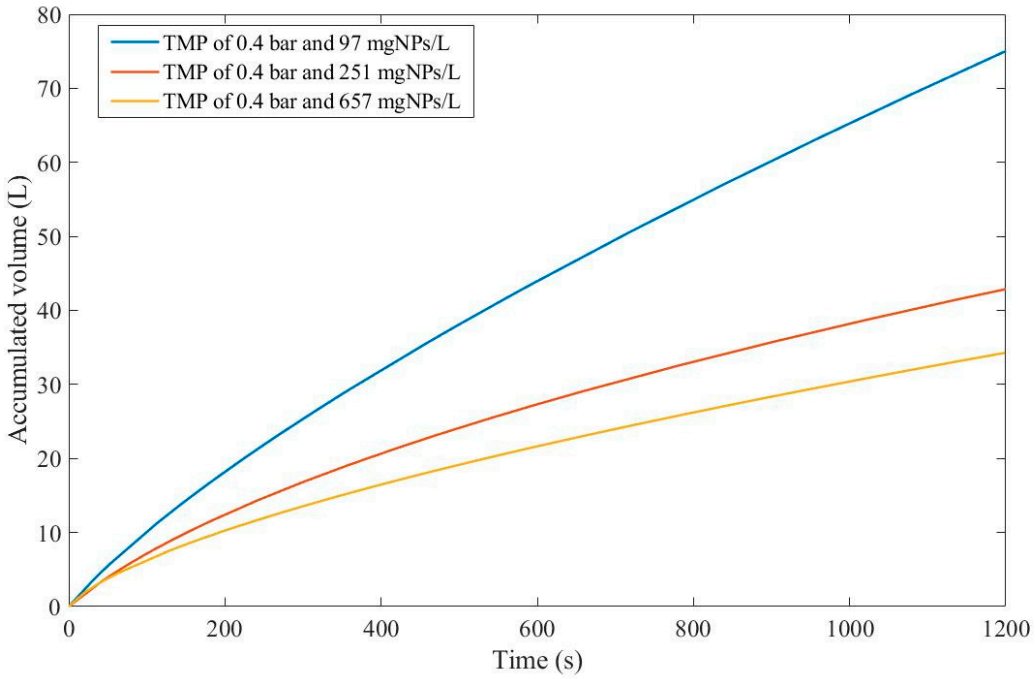

Figure 5. The accumulated volume calculated through the EHM for dead-end ultrafiltration of nanoparticles from polishing wastewater at 0.4bar assuming $A = 1.00\ m^2$

Even though j_0 for 657 mgNPs/L is greater than j_0 for 97 mgNPs/L, Figure 5 shows that the accumulated volume obtained through a concentration of 97 mgNPs/L is far greater than for higher concentrations. This implies that the effects of fouling are more pronounced for higher concentrations as demonstrated through EHM half-life. Therefore, we can conclude that, in Example 6, a 3rd-degree pore-blocking mechanism at lower concentrations for dead-end ultrafiltration of nanoparticles at 0.4 bar is advantageous.

4. Discussion

4.1. How the blocking mechanism changes with membrane types and pre-treatments

In the same filtration conditions, different membrane types also have different blocking mechanisms, such as shown in **Example 1**, where HPI and HPO membranes behaved differently. This behavior was recurrent in Example 1, where changes to both the foulant and the fluid caused changes in fouling for both HPI and HPO. Other membrane properties also influence the blocking mechanism, such as shown in Example 2, where the same type of ceramic membrane performed differently due to differences in mean pore radius obtained through volume mercury penetration (r_p), hydraulic permeability (L_h) and porosity (ε). Membrane usage also plays a big role, since multiple fouling stages also change the blocking mechanism. The use of coatings also has effects on the pore-blocking mechanism, such as shown in Example 5.

A common factor in Examples 1, 2, and 5 is the changes in the interactions between the foulant and the membrane itself. HPI and HPO have different van der Walls interactions with both the foulant and the fluid, the use of coagulants and additives changes the size distribution of particles, different mean pore radius influences the membrane's selectivity, and changes to the membrane's surface interfere also change how fouling layers behave when in contact with the membrane. Therefore, given all possible changes that can be made to an experimental setup, the influence of these changes in the pore-blocking mechanism is very situation-specific.

For instance, in Example 1 the experimental conditions that maximized EHM half-life were the use of both additives with the HPI membrane, changing the pore-blocking mechanism from a mixture of cake formation and a 3rd-degree mechanism to a mainly 3rd-degree. In contrast, in Example 5 the coated membrane maximized EHM half-life by changing the pore-blocking mechanism from a mixture of intermediate blocking and cake formation to mainly cake formation.

4.2. How the blocking mechanism changes with TMP, CFR, CFV, and matter concentration

The effects of TMP in the pore-blocking mechanism seem to vary in intensity, as shown in Examples **Example 2**, **Example 3**, and **Example 4**. In Example **2** an increase in TMP for CM05 causes a decrease in the value of P, changing the blocking mechanism from manly cake formation to mainly intermediate blocking. In Example 3 at a CFR of 14 L/min, an increase in TMP leads to a slight decrease in P, meanwhile at CFRs of 28 and 40 L/min P seems to slightly increase. In contrast, in Example 4 a smaller increase in TMP leads to P nearly dropping down by half. In both Examples Example **2** and Example **4**, increasing TMP seems to decrease P. The changes in TMP applied in Example 3 do not cause significant changes in P, therefore we can suggest that P is inversely proportional to TMP, however, further use of the EHM is necessary to confirm this statement.

Changes in CFR, and consequently CFV, seem to vary with TMP. In Example 3, at a TMP of 21 kPa, an increase in CFR leads to a decrease in P. This bahaviour changes for TMPs of 35 and 104 kPa, where an increase in CFR leads to a decrease in P. The same type of mixed behavior has been identified in Example 4, where an increase in CFV from 0.75 to 1.50 m/s leads to a decrease in P, yet a further increase from 1.50 to 3.00 m/s causes an increase.

Similar non-linear effects can be found in changes in concentration, such as in Example 6. An increase in nanoparticle concentration from 97 to 251 mgNPs/L decreases P, changing the blocking mechanism from a 3rd-degree to cake formation. Yet further increase from 251 to 657 mgNPs/L increases P, changing the blocking mechanism from cake formation to a mixture of cake formation and a 3rd-degree blocking mechanism.

Taking into account Examples **Example 2**, **Example 3**, **Example 4**, and **Example 6**, we have shown that the same types of changes in the operating conditions of different filtration

systems lead to vastly different fouling behavior and pore-blocking mechanisms. Therefore, the use of P as a tool to better understand fouling in membranes needs to be accompanied by auxiliary variables that indicate different performances, such as the EHM half-life, the accumulated volume, matter concentration measurements, and so on.

4.3. Higher-degree and mixed pore-blocking mechanisms

In Examples 1, 2, 4, 5, and 6 we have found optimal values of $\boldsymbol{P}$ that are higher than 2nd-degree blocking (cake formation). In other words, there are values of $\boldsymbol{P > 2}$. Through its connection to n, there seem to be not only values of n between the original four blocking mechanisms ($n = 0,1,3/2,2$) but also values where $n < 0$. The standard physical interpretation is for these exact values, such that complete blocking is $n = 2$, intermediate blocking is $n = 1$, standard blocking is $n = 3/2$, and cake formation $n = 0$. It is possible to interpret the values in between (i.e., $n = 0.75$) as a mixture between the pore-blocking mechanisms (i.e., cake formation and intermediate blocking). This interpretation has been used in all Examples. The physical interpretation for values of $n < 0$ (or $P > 2$) requires more experimental work to fully understand what these new possible pore-blocking mechanisms look like and how they contribute to membrane fouling as a whole.

4.4. Fouling mitigation, optimal filtration conditions, and physical representative use of the EHM

Given Eq. 20 and Eq. 22 from Theorems 1 and 3, both the EHM half-life and the accumulated volume increase with P and decreases with k, therefore, to increase the half-life of the membrane it is possible to apply many strategies that increase the degree of the pore-blocking mechanism, as the ones applied in Examples 1-6. It is important to point out that given the non-linearity of the conditions, such as shown in Section 4.2., optimizations should follow a systematic approach, perhaps given by experimental design tools and statistical analysis. We have shown in Example 4 that the EHM can be used to predict interpolated values, yet extrapolations can lead to inconclusive results. Therefore, the representative use of the model depends on the data used for the model fitting.

5. Conclusions

- The Hermia model can be used for any real values of n and k for equal or approximate entrance and exit densities.
- The permeate flux j is given by a power law dependent on the value of n for any real $n \neq 2$.
- The permeate flux j is given by an exponential function when $n = 2$.
- The accumulated volume as a function of time follows the same type of ODE expressed by time as a function of the accumulated volume.
- The mass flux $N(t)$ behaves similarly to the permeate flux j.
- There is a correction term for the difference between the entrance and exit densities that scales up j_0 such that the continuity equation is obeyed.
- For $n \neq 2$, j will become a constant value if P tends to infinity.
- P is related to n, since $P = n - 2$.
- Since n is a continuous quantity, there are solutions between the four original discrete values, which can be physically interpreted as the existence of new types of blocking mechanisms.
- The fouling curve $\delta(t)$ is also given by a power law dependent on P for any real $P \neq 0$.
- The fouling curve $\delta(t)$ is also given by an exponential function when $P = 0$,
- When $P \to \infty$, $P \to -\infty$ or $P = -1$, the fouling curves given by $\delta(t)$ behave linearly.
- There is one and only one unique fouling profile $\delta(t)$ for every real value P;
- Ultrafiltration and microfiltration can be modeled.
- The EHM performed consistently better than the four original pore-blocking mechanisms in all examples.

- The effects of membrane composition, solution nature, TMP, CFR, and CFV impact greatly the values of P and k, therefore the fouling behavior is situation-specific and P and k may vary differently with the same variable in different cases.

Author Contributions: Gustavo Leite Dias Pereira: Conceptualization, Methodology, Investigation, Writing – Original Draft. **Lucio Cardoso-Filho:** Supervision, Project administration, Resources. **Veeriah Jegatheeesan:** Validation, Writing – Review, and Editing. **Reginaldo Guirardello:** Validation, Writing – Review, and Editing.

Funding: This research did not receive any financial support or material aid of any kind.

Institutional Review Board Statement: Not applicable.

Data Availability Statement: Not applicable.

Acknowledgments: We thank the State University of Maringa, the State University of Campinas, and the RMIT for their help with writing and reviewing the proof.

Conflicts of Interest: The authors declare that they have no known competing financial interests or personal relationships that could have appeared to influence the work reported in this paper.

Appendix A: Proof of Theorem 1

Taking all the equations presented in Section 2, it is possible to take the control volume from Section 2.1 and apply the continuity equation (Eq. 6). By assuming that the system has uniform entrances and exits, the surface integral can be reduced to:

$$\iint_{CS} \rho\vec{j} \cdot d\vec{A} = \sum_{CS} \rho_i j_i A_i \qquad \text{Eq. 23}$$

For the present system, there are two sources of flux, the entrance, and the exit. As a result, this sum is given by:

$$\sum_{CS} \rho_i j_i A_i = \rho_{exit} j(t) A_{exit} - \rho_{ent} j_0 A_{ent} \qquad \text{Eq. 24}$$

By the definition of flux given in Eq. 10, $N_0 = \rho_{in} j_0$ and $N(t) = \rho_{out} j(t)$. Since the control volume has a constant area, $A_{exit} = A_{ent} = A$. Therefore:

$$\sum_{CS} \rho_i j_i A_i = A \cdot (N(t) - N_0) \qquad \text{Eq. 25}$$

Thus, the surface integral of the Continuity Equation is simplified to:

$$\iint_{CS} \rho\vec{j} \cdot d\vec{A} = A \cdot (N(t) - N_0) \qquad \text{Eq. 26}$$

As for the volume integral, since the control volume itself is a porous solid with a constant density ρ_s, a base area A and thickness $\delta(t)$:

$$\iiint_{CV} \rho d\forall = \rho_s \forall = \rho_s \cdot A \cdot \delta(t) \qquad \text{Eq. 27}$$

So:

$$\frac{\partial}{\partial t} \iiint_{CV} \rho d\forall = \rho_s \cdot A \cdot \frac{d\delta(t)}{dt} \qquad \text{Eq. 28}$$

Going back to the Continuity Equation:

$$\rho_s \cdot A \cdot \frac{d\delta(t)}{dt} + A \cdot (N(t) - N_0) = 0$$

Preprints (www.preprints.org) | NOT PEER-REVIEWED | Posted: 5 January 2023 doi:10.20944/preprints202206.0187.v2

Peer-reviewed version available at Membranes 2023, 13, 290; doi:10.3390/membranes13030290

If $k_1 = \rho_s$, then:

$$N(t) = N_0 - k_1 \cdot \frac{d\delta(t)}{dt} \qquad \text{Eq. 29}$$

According to Eq. 7, for a real constant k_2:

$$\frac{d^2t}{dV^2} = k_2 \left(\frac{dt}{dV}\right)^n \qquad \text{Eq. 30}$$

Using the first property presented in Eq. 8, it is possible to write dt/dV in terms of dV/dt. Therefore:

$$\left(\frac{dt}{dV}\right)_{V^*} = \left[\left(\frac{dV}{dt}\right)_{t^*}\right]^{-1} \qquad \text{Eq. 31}$$

For $V(t^*) = V^*$. Now using the second property from the same Section, it is possible to write d^2t/dV^2 in terms of dV^2/dt^2. Thus, Eq. 30 can be rewritten as:

$$\left(\frac{d^2t}{dV^2}\right)_{V^*} = -\left(\frac{d^2V}{dt^2}\right)_{t^*} \cdot \left[\left(\frac{dt}{dV}\right)_{V^*}\right]^3$$

Using Eq. 31:

$$\left(\frac{d^2t}{dV^2}\right)_{V^*} = -\left(\frac{d^2V}{dt^2}\right)_{t^*} \cdot \left[\left(\frac{dV}{dt}\right)_{t^*}\right]^{-3} \qquad \text{Eq. 32}$$

Applying Eq. 31 and Eq. 32 to the Hermia model:

$$\left[-\left(\frac{d^2V}{dt^2}\right)_{t^*} \cdot \left[\left(\frac{dV}{dt}\right)_{t^*}\right]^{-3}\right] = k_2 \cdot \left\{\left[\left(\frac{dV}{dt}\right)_{t^*}\right]^{-1}\right\}^n$$

$$\left(\frac{d^2V}{dt^2}\right)_{t^*} = k_3 \left[\left(\frac{dV}{dt}\right)_{t^*}\right]^{3-n}$$

If $m = 3 - n$ and k_3 is another real constant, then:

$$\left(\frac{d^2V}{dt^2}\right)_{t^*} = k_3 \left[\left(\frac{dV}{dt}\right)_{t^*}\right]^m$$

Since both of these derivatives have the same domain of t, then for any t^*, this ODE is valid, therefore it is possible to remove the subscript.

$$\frac{d^2V}{dt^2} = k_3 \left[\left(\frac{dV}{dt}\right)\right]^m \qquad \text{Eq. 33}$$

It is important to note that both Eq. 30 and Eq. 33 are analogous, which means that both functions $t(V)$ and $V(t)$ are solutions of the same family of differential equations. By the definition of accumulated volume presented in Eq. 11, it is possible to use Eq. 29, such that;

$$V(t) = \frac{A}{\rho_{exit}} \int_0^t \left[N_0 - k_1 \frac{d\delta(t)}{dt}\right] dt$$

By the integral property presented in Eq. 12:

$$\int_0^t \left[\frac{d\delta(t)}{dt}\right] dt = \delta(t) - \delta(0)$$

Since there is no mass accumulated in the control volume at $t = 0$, then $\delta(0) = 0$. As a result:

$$V(t) = \frac{A}{\rho_{exit}} [N_0 \cdot t - k_1 \delta(t)] \qquad \text{Eq. 34}$$

Differentiating $V(t)$ twice:

Preprints (www.preprints.org) | NOT PEER-REVIEWED | Posted: 5 January 2023 doi:10.20944/preprints202206.0187.v2

Peer-reviewed version available at Membranes 2023, 13, 290; doi:10.3390/membranes13030290

$$\frac{dV}{dt} = \frac{A}{\rho_{exit}}\left[N_0 - k_1\frac{d\delta(t)}{dt}\right] \qquad \text{Eq. 35}$$

$$\frac{d^2V}{dt^2} = -k_1\frac{A}{\rho_{exit}}\cdot\frac{d^2\delta(t)}{dt^2} \qquad \text{Eq. 36}$$

With these derivatives, it is possible to rewrite Eq. 33, such that:

$$-k_1\frac{A}{\rho_l}\cdot\frac{d^2\delta(t)}{dt^2} = k_3\left[\frac{A}{\rho_{exit}}\left[N_0 - k_1\frac{d\delta(t)}{dt}\right]\right]^m$$

For another real constant k_4:

$$\frac{d^2\delta(t)}{dt^2} = k_4\left[N_0 - k_1\frac{d\delta(t)}{dt}\right]^m \qquad \text{Eq. 37}$$

Reducing Eq. 37 further with Eq. 29:

$$\frac{d^2\delta(t)}{dt^2} = k_4[N(t)]^m \qquad \text{Eq. 38}$$

By differentiating Eq. 29:

$$\frac{dN(t)}{dt} = -k_1\frac{d^2\delta(t)}{dt^2} \qquad \text{Eq. 39}$$

Therefore, Eq. 38 can be simplified further to:

$$\frac{dN(t)}{dt} = k_5[N(t)]^m \qquad \text{Eq. 40}$$

Such that k_5 is another real constant. Now, by applying the separation of variables method [17]:

$$[N(t)]^{-m}dN(t) = k_5dt$$

As a result, for $m \neq 1$:

$$\int_{N(0)}^{N(t)}[N(t)]^{-m}dN(t) = \int_0^t k_5dt$$

$$\left[\frac{[N(t)]^{(1-m)}}{(1-m)}\right]_{N(0)}^{N(t)} = [k_5t]_0^t$$

$$\frac{1}{(1-m)}\{[N(t)]^{1-m} - [N(0)]^{1-m}\} = k_5t$$

$$[N(t)]^{1-m} = [N(0)]^{1-m} + (1-m)k_5t$$

If $P = -(1-m)$:

$$[N(t)]^{-P} = [N(0)]^{-P} - P\cdot k_5\cdot t$$

And $-Pk_5 = k_6$:

$$[N(t)]^{-P} = [N(0)]^{-P} + k_6\cdot t$$

Since there is no mass accumulated at the beginning of the filtration experiment ($\delta(0) = 0$), both N_0 and $N(0)$ are equal. Therefore:

$$[N(t)]^{-P} = [N_0]^{-P} + k_6\cdot t \qquad \text{Eq. 41}$$

It is important to notice that Eq. 30 is similar to the original equations used in the Hermia model. It is also important to highlight that both P and k_6 can assume any real values, as long as $P \neq 0$. By using the flux definition presented in Section 2.4.

Preprints (www.preprints.org) | NOT PEER-REVIEWED | Posted: 5 January 2023 doi:10.20944/preprints202206.0187.v2

Peer-reviewed version available at Membranes 2023, 13, 290; doi:10.3390/membranes13030290

$$[\rho_{exit} j(t)]^{-P} = [\rho_{ent} j_0]^{-P} + k_6 \cdot t$$

Thus, if k_7 is another real constant:

$$[j(t)]^{-P} = \left[\frac{\rho_{ent}}{\rho_{exit}}\right]^{-P} \cdot j_0^{-P} + k_7 \cdot t \quad \text{Eq. 42}$$

As a result, Eq. 31 closely resembles the power law used in the Hermia fouling model. However, the additional term $[\rho_{ent}/\rho_{exit}]^{-P}$ correctly scales up j_0 such that the right-hand side of Eq. 31 agrees with the Continuity Equation. In special cases where the density of the permeate is close to the original density ($\rho_{exit} \to \rho_{ent}$), the correction term $[\rho_{ent}/\rho_{exit}]^{-P} \to 1$. If that is the case, $[j(t)]^{-P}$ can be approximated by:

$$[j(t)]^{-P} \approx j_0^{-P} + k_7 \cdot t$$

Therefore, for a new constant k:

$$\left[\frac{j(t)}{j_0}\right]^{P} \approx \frac{1}{(1 + k \cdot t)} \quad \text{Eq. 43}$$

For the special case, when $m = 1$:

$$\int_{N_0}^{N(t)} \frac{1}{N(t)} dN(t) = \int_0^t k_5 dt$$

$$\ln\left[\frac{N(t)}{N_0}\right] = k_5 t$$

$$N(t) = N_0 \exp(k_5 t)$$

If $k = -k_5$, then:

$$N(t) = N_0 \exp(-k \cdot t) \quad \text{Eq. 44}$$

Since Eq. 44 has an exponential function multiplying N_0, and k can assume positive values (or $k_5 < 0$), when $m = 1$, the system can behave with a classical drop for $N(t)$. Applying again the flux definition presented in Eq. 10:

$$\rho_{exit} j(t) = \rho_{ent} j_0 \, exp(-k \cdot t)$$

$$j(t) = j_0 \left[\frac{\rho_{ent}}{\rho_{exit}}\right] exp(-k \cdot t) \quad \text{Eq. 45}$$

For the same reasons as before, if $\rho_{exit} \to \rho_{ent}$, $[\rho_{ent}/\rho_{exit}] \to 1$ and $j(t)$ can be approximated by:

$$j(t) \approx j_0 \, exp(-k \cdot t) \quad \text{Eq. 46}$$

It is possible to conclude that $P = 2 - n$. By using the four original discrete values of $n = 2, 1, 3/2, 0$, $P = 0, 1, 1/2, 2$, which are exactly the respective exponents of j in Eq. 1-4. Thus, through Eq. 43 and Eq. 46, it is possible to reproduce the entire Hermia model. Since Eq. 43 was obtained for any real $n \neq 2$ and Eq. 46 was obtained for $n = 2$, these equations form a model that can be used for any real n, which widens the usefulness of the Hermia model considerably. Consequently, there are also values of n between the four original discrete values, which can be physically interpreted as the existence of new types of fouling mechanisms in membranes.

Appendix B: Proof of Theorem 2

It is also possible to deduce how the fouling profile should change with P, given by the function $\delta(t)$. Through Eq. 9 and 18, it is possible to show that:

$$\left[\frac{j(t)}{j_0}\right] = \left[\frac{\rho_{ent}}{\rho_{exit}}\right] - k_{10}\frac{d\delta(t)}{dt} \qquad \text{Eq. 47}$$

For another real constant k_{10}. For the case of $P \neq 0$, the profile of $j(t)$ is given by Eq. 42. Taking this equation and dividing both sides by j_0^{-P}:

$$\left[\frac{j(t)}{j_0}\right]^{-P} = \left[\frac{\rho_{ent}}{\rho_{exit}}\right]^{-P} + k_7 t \qquad \text{Eq. 48}$$

Since k_7/j_0^{-P} is still a constant in Eq. 37, the same constant will be used. Therefore, by substituting Eq. 47 into Eq. 48:

$$\left[\left[\frac{\rho_{ent}}{\rho_{exit}}\right] - k_{10}\frac{d\delta(t)}{dt}\right]^{-P} = \left[\frac{\rho_{ent}}{\rho_{exit}}\right]^{-P} + k_7 t$$

$$\left[\frac{\rho_{ent}}{\rho_{exit}}\right] - k_{10}\frac{d\delta(t)}{dt} = \left(\left[\frac{\rho_{ent}}{\rho_{exit}}\right]^{-P} + k_7 t\right)^{-1/P}$$

$$-k_{10}\frac{d\delta(t)}{dt} = \left(\left[\frac{\rho_{ent}}{\rho_{exit}}\right]^{-P} + k_7 t\right)^{-\frac{1}{P}} - \left[\frac{\rho_{ent}}{\rho_{exit}}\right]$$

If k_{11} and k_{12} are other real constants, then:

$$\frac{d\delta(t)}{dt} = k_{11}\left(\left[\frac{\rho_{ent}}{\rho_{exit}}\right]^{-P} + k_7 t\right)^{-\frac{1}{P}} + k_{12}$$

$$\frac{d\delta(t)}{dt} = \left(k_{11}^{-P}\left[\frac{\rho_{ent}}{\rho_{exit}}\right]^{-P} + k_{11}^{-P}k_7 t\right)^{-\frac{1}{P}} + k_{12}$$

Thus, if $k_{13} = k_{11}^{-P}[\rho_{ent}/\rho_{exit}]^{-P}$ and $k_{14} = k_{11}^{-P}k_7$:

$$\frac{d\delta(t)}{dt} = (k_{13} + k_{14}t)^{-\frac{1}{P}} + k_{12} \qquad \text{Eq. 49}$$

Now, by applying the separation of variables method in Eq. 49:

$$\int_{\delta(0)}^{\delta(t)} d\delta(t) = \int_0^t [(k_{13} + k_{14}t)^{-\frac{1}{P}} + k_{12}]dt$$

Since:

$$\int_{\delta(0)}^{\delta(t)} d\delta(t) = \delta(t) - \delta(0)$$

And $\delta(0) = 0$, then:

$$\delta(t) = \int_0^t [(k_{13} + k_{14}t)^{-\frac{1}{P}} + k_{12}]dt \qquad \text{Eq. 50}$$

By integrating Eq. 39 with respect to t:

Preprints (www.preprints.org) | NOT PEER-REVIEWED | Posted: 5 January 2023 doi:10.20944/preprints202206.0187.v2

Peer-reviewed version available at Membranes 2023, 13, 290; doi:10.3390/membranes13030290

$$\delta(t) = \left[\frac{1}{k_{14}}\frac{(k_{13}+k_{14}t)^{-\frac{1}{P}+1}}{\left(-\frac{1}{P}+1\right)} + k_{12}t\right]_0^t$$

$$\delta(t) = \frac{1}{k_{14}}\left[\frac{(k_{13}+k_{14}t)^{-\frac{1}{P}+1} - k_{13}^{-\frac{1}{P}+1}}{\left(-\frac{1}{P}+1\right)}\right] + k_{12}t$$

It is possible to further reduce this equation by distributing the terms $1/k_{14}$ and $\left(-\frac{1}{P}+1\right)$. By doing that, it should be possible to regroup the constants inside the brackets of $(k_{13}+k_{14}t)^{-\frac{1}{P}+1}$. If:

$$k_{15} = \frac{k_{13}}{\left(k_{14}\cdot\left(-\frac{1}{P}+1\right)\right)^{-\frac{1}{P}+1}}$$

$$k_{16} = \frac{k_{14}}{\left(k_{14}\cdot\left(-\frac{1}{P}+1\right)\right)^{-\frac{1}{P}+1}}$$

$$k_{17} = \frac{-k_{13}^{-\frac{1}{P}+1}}{k_{14}\cdot\left(-\frac{1}{P}+1\right)}$$

Then:

$$\delta(t) = (k_{15}+k_{16}t)^{-\frac{1}{P}+1} + k_{17} + k_{12}t \quad \text{Eq. 51}$$

By applying $\delta(0) = 0$ in Eq. 51, it can be found that:

$$k_{17} = -k_{15}^{-\frac{1}{P}+1}$$

As a result, Eq. 51 can be further reduced to:

$$\delta(t) = (k_{15}+k_{16}t)^{-\frac{1}{P}+1} - k_{15}^{-\frac{1}{P}+1} + k_{12}t \quad \text{Eq. 52}$$

For the case of $P = 0$, through Eq. 46 and Eq. 47, it is possible to show that:

$$\left[\frac{\rho_{ent}}{\rho_{exit}}\right]exp(-k_9 t) = \left[\frac{\rho_{ent}}{\rho_{exit}}\right] - k_{10}\frac{d\delta(t)}{dt}$$

Dividing both sides by $[\rho_{ent}/\rho_{exit}]$:

$$exp(-k_9 t) = 1 - k_{10}\left[\frac{\rho_{exit}}{\rho_{ent}}\right]\frac{d\delta(t)}{dt}$$

If $1/k_{18} = -k_{10}[\rho_{exit}/\rho_{ent}]$, then:

$$exp(-k_9 t) = 1 + \frac{1}{k_{18}}\frac{d\delta(t)}{dt}$$

Therefore:

$$\frac{d\delta(t)}{dt} = k_{18}[exp(-k_9 t) - 1] \quad \text{Eq. 53}$$

Preprints (www.preprints.org) | NOT PEER-REVIEWED | Posted: 5 January 2023 doi:10.20944/preprints202206.0187.v2

Peer-reviewed version available at Membranes 2023, 13, 290; doi:10.3390/membranes13030290

Now, by applying the separation of variables method in Eq. 53 [16]

$$\int_{\delta(0)}^{\delta(t)} d\delta(t) = k_{18} \int_0^t [exp(-k_9 t) - 1]\, dt$$

$$\delta(t) = k_{18} \left[\frac{1}{-k_9} exp(-k_9 t) - t \right]_0^t$$

$$\delta(t) = -\frac{k_{18}}{k_9} [exp(-k_9 t) - 1] - k_{18} t$$

If $k_{19} = -k_{18}/k_9$ and $k_{20} = -k_{18}$, then:

$$\delta(t) = k_{19}[exp(-k_9 t) - 1] + k_{20} t \quad \text{Eq. 54}$$

As a result, with Eq. 52 and Eq. 54, it is possible to construct a fouling model for every real value of P, such that:

$$\delta(t) = \begin{cases} (k_{15} + k_{16} t)^{-\frac{1}{P}+1} - k_{15}^{-\frac{1}{P}+1} + k_{12} t, & P \neq 0 \\ k_{19}[\exp(-k_9 t) - 1] + k_{20} t, & P = 0 \end{cases} \quad \text{Eq. 55}$$

It is important to notice that the different fouling profiles δ are given by the exponent $-1/P + 1$. Therefore, by analyzing this exponent, it is possible to conclude the fouling profiles as well. By taking the limit as $P \to \infty$,$-1/P \to 0$:

$$\delta(t) = (k_{15} + k_{16} t)^{0+1} - k_{15}^{0+1} + k_{12} t$$

$$\delta(t) = (k_{16} + k_{12}) t$$

Now, by taking the limit as $P \to -\infty$, $-1/P \to 0$:

$$\delta(t) = (k_{15} + k_{16} t)^{0+1} - k_{15}^{0+1} + k_{12} t$$

$$\delta(t) = (k_{16} + k_{12}) t$$

Therefore, for both $P \to \infty$ and $P \to -\infty$, the result is a linear curve. The same behavior can be seen when $P = 1$, since:

$$\delta(t) = (k_{15} + k_{16} t)^{1-1} - k_{15}^{1-1} + k_{12} t$$

$$\delta(t) = k_{12} t$$

For positive values of P, the exponent $-1/P + 1$ is always smaller than 1, in contrast for negative values of P, $-1/P + 1$ is always larger than 1. Consequently, there is one and only one unique fouling profile $\delta(t)$ for every real value P.

Appendix C: Proof of Theorem 3

$$\frac{dV}{dt} = j(t) \cdot A$$

$$dV = j(t) \cdot A \cdot dt$$

For $P \neq 0$:

$$\left[\frac{j(t)}{j_0} \right]^P \approx \frac{1}{(1 + k \cdot t)}$$

Therefore:

$$dV = j_0 \cdot A \cdot \left[\frac{1}{(1+k\cdot t)}\right]^{\frac{1}{P}} \cdot dt$$

$$\int_{V(0)}^{V(t)} dV = j_0 \cdot A \cdot \int_0^t \left[\frac{1}{(1+k\cdot t)}\right]^{\frac{1}{P}} \cdot dt$$

$$V(t) - V(0) = j_0 \cdot A \cdot \int_0^t [(1+k\cdot t)]^{-\frac{1}{P}} \cdot dt$$

Since there is no permeate at $t = 0$, $V(0) = 0$:

$$V(t) = j_0 \cdot A \cdot \left[\frac{[(1+k\cdot t)]^{1-\frac{1}{P}}}{k\cdot\left(1-\frac{1}{P}\right)}\right]_0^t$$

$$V(t) = \frac{j_0 \cdot A}{k\left(1-\frac{1}{P}\right)}([1+k\cdot t]^{\left(1-\frac{1}{P}\right)} - 1)$$

For $P = 0$:

$$\frac{j(t)}{j_0} \approx \exp(-k\cdot t)$$

Thus:

$$\int_{V(0)}^{V(t)} dV = j_0 \cdot A \cdot \int_0^t \exp(-k\cdot t)\cdot dt$$

$$V(t) = j_0 \cdot A \cdot \left[-\frac{\exp(-k\cdot t)}{k}\right]_0^t$$

$$V(t) = \frac{j_0 \cdot A}{k} \cdot [1 - \exp(-k\cdot t)]$$

Therefore:

$$V(t) = \begin{cases} \frac{j_0 \cdot A}{k\left(1-\frac{1}{P}\right)}([1+k\cdot t]^{\left(1-\frac{1}{P}\right)} - 1), & P \neq 0 \\ \frac{j_0 \cdot A}{k}[1 - exp(-k\cdot t)], & P = 0 \end{cases}$$

Appendix D: Complementary Figures

Example 1:

Preprints (www.preprints.org) | NOT PEER-REVIEWED | Posted: 5 January 2023 doi:10.20944/preprints202206.0187.v2

Peer-reviewed version available at Membranes 2023, 13, 290; doi:10.3390/membranes13030290

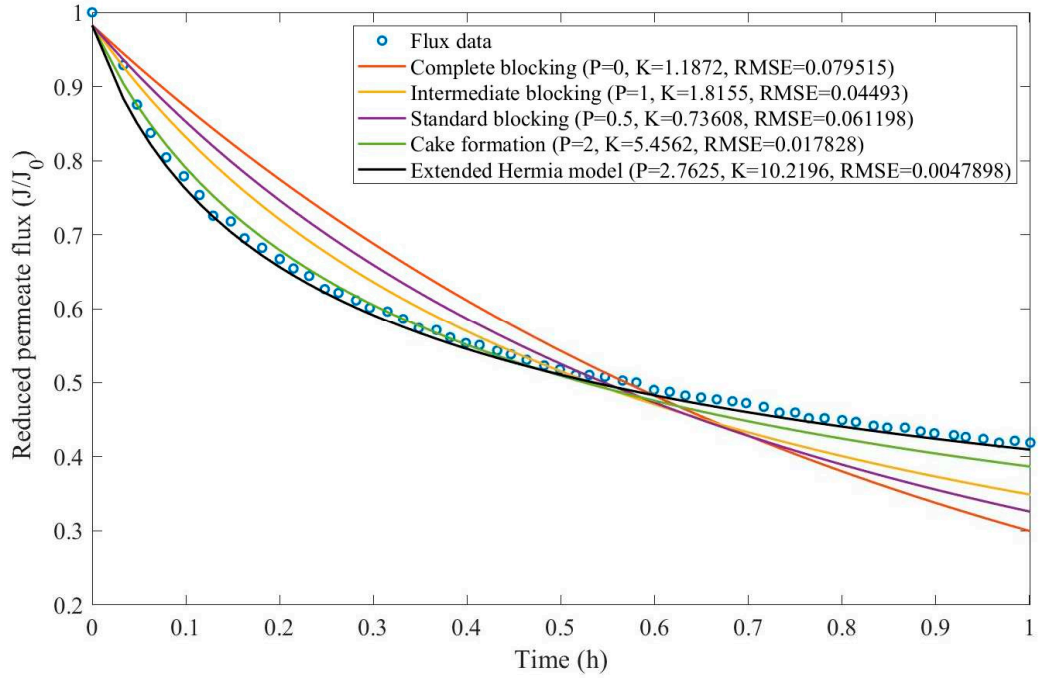

Figure D 1. Model fitting for HPI ultrafiltration considering the four original pore-blocking mechanisms and the extended Hermia model (15)

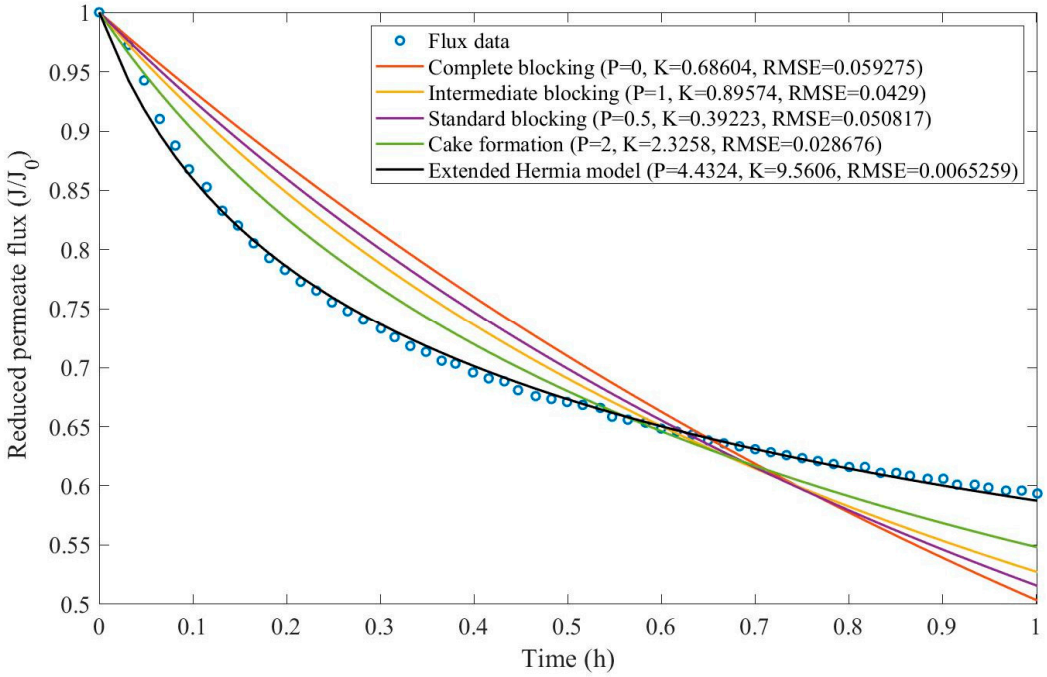

Figure D 2. Model fitting for Coagulant 140mg/L + HPI ultrafiltration considering the four original pore-blocking mechanisms and the extended Hermia model (15)

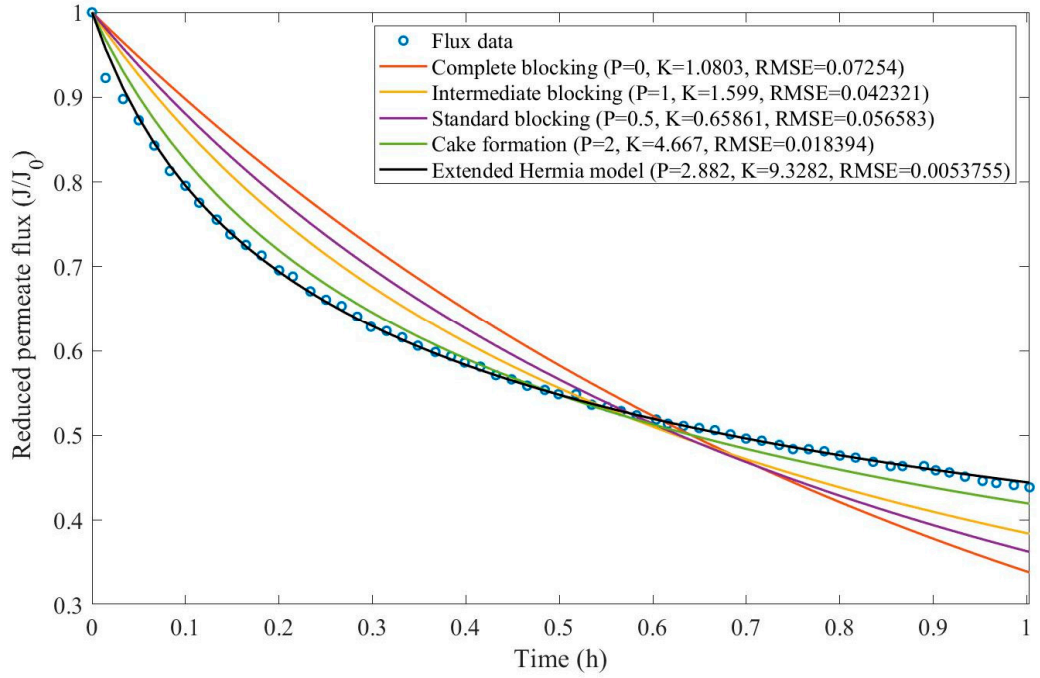

Figure D 3. Model fitting for MIEX 12mL/L + HPI ultrafiltration considering the four original pore-blocking mechanisms and the extended Hermia model (15)

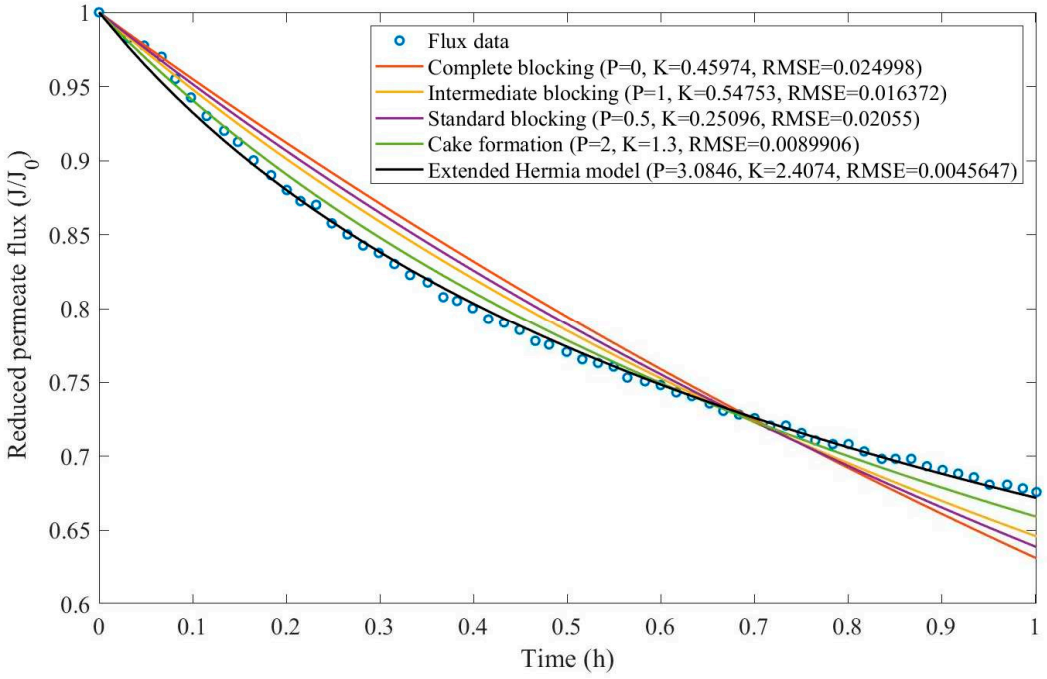

Figure D 4. Model fitting for MIEX 12mL/L + Coagulant 40mg/L + HPI ultrafiltration considering the four original pore-blocking mechanisms and the extended Hermia model (15)

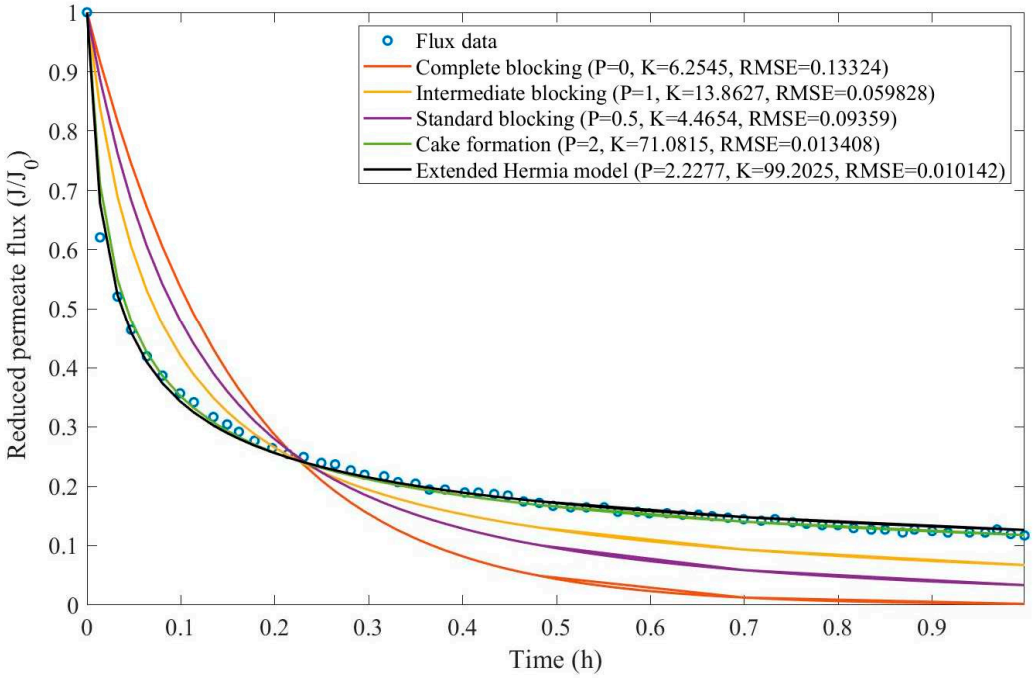

Figure D 5. Model fitting for HPO ultrafiltration considering the four original pore-blocking mechanisms and the extended Hermia model (15)

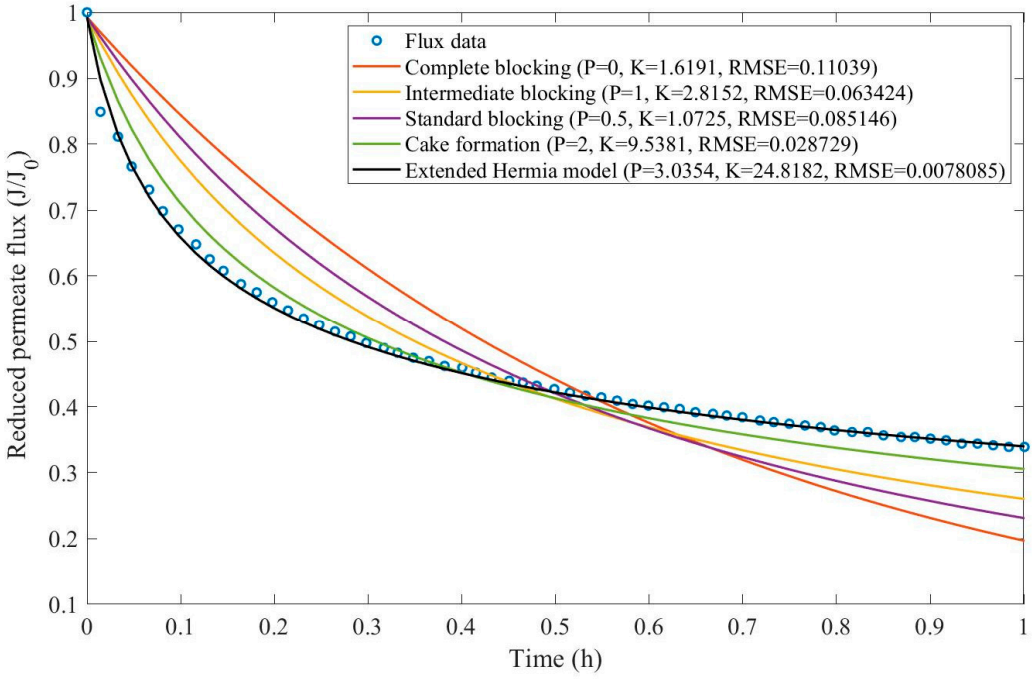

Figure D 6. Model fitting for Coagulant 140mg/L + HPO ultrafiltration considering the four original pore-blocking mechanisms and the extended Hermia model (15)

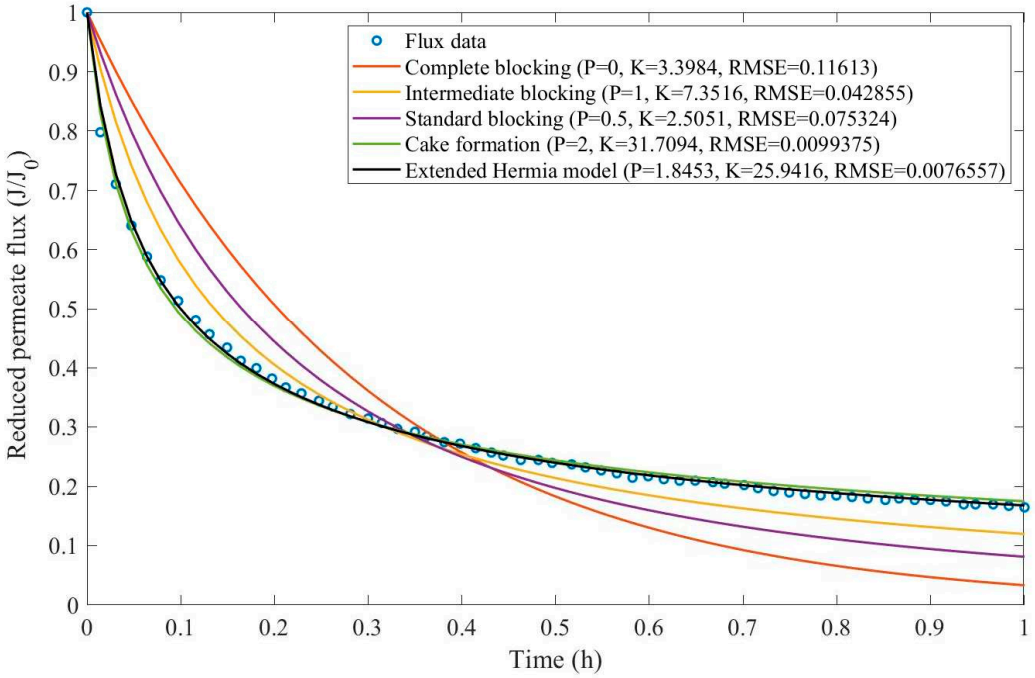

Figure D 7. Model fitting for MIEX 12mL/L + HPO ultrafiltration considering the four original pore-blocking mechanisms and the extended Hermia model (15)

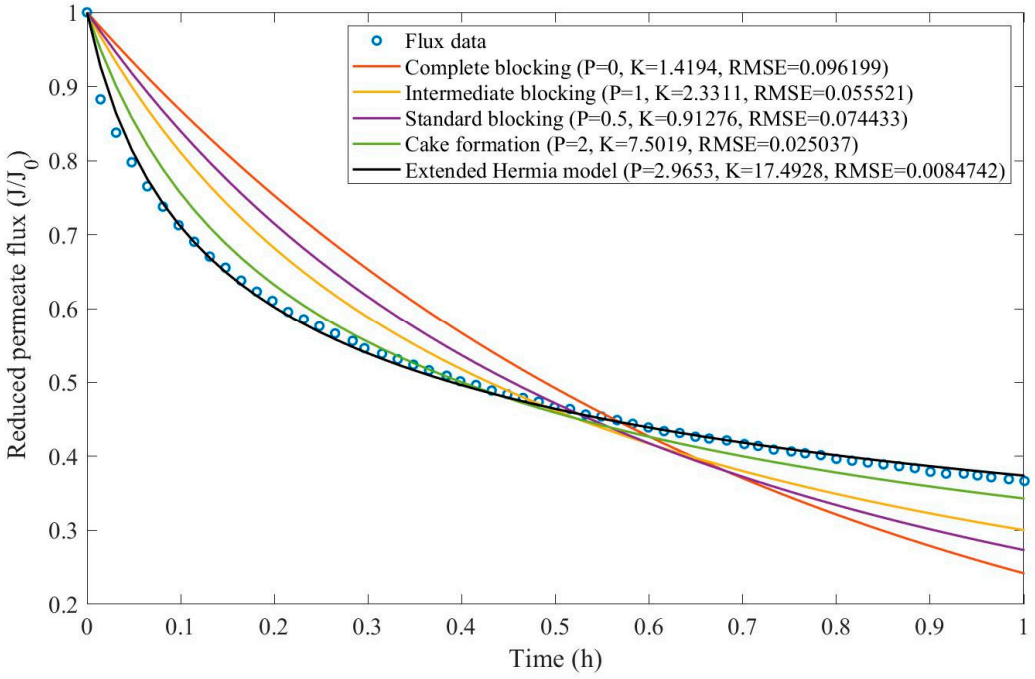

Figure D 8. Model fitting for MIEX 12mL/L + Coagulant 40mg/L + HPO ultrafiltration considering the four original pore-blocking mechanisms and the extended Hermia model (15)

Example 2:

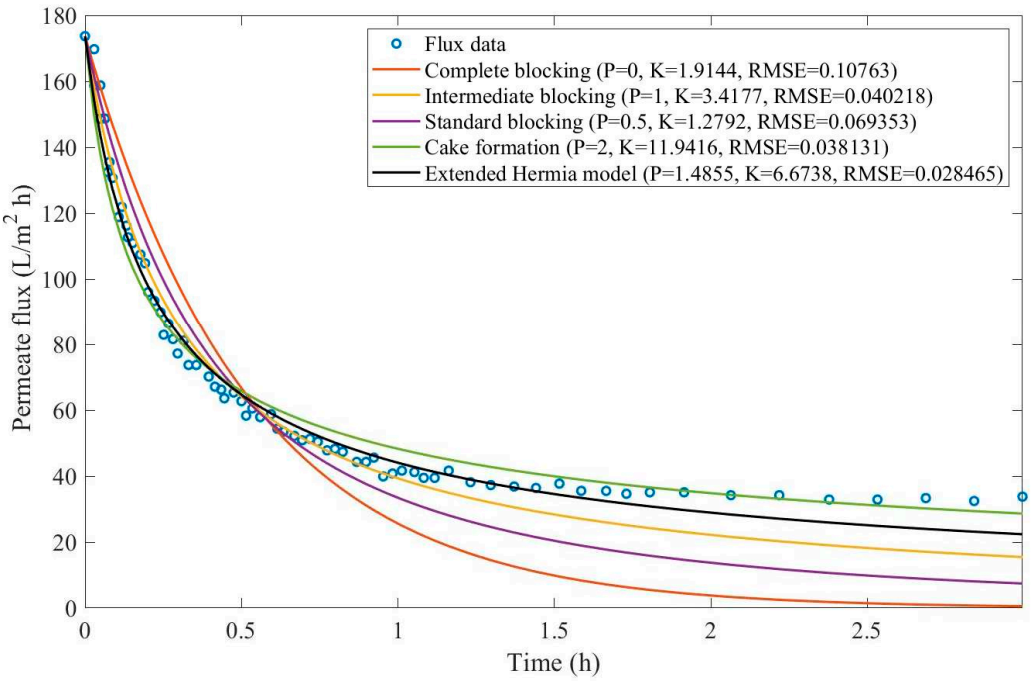

Figure D 9. Model fitting for corn syrup microfiltration with CM08 at 0.5 m/s and 50kPa considering the four original pore-blocking mechanisms and the extended Hermia model (16)

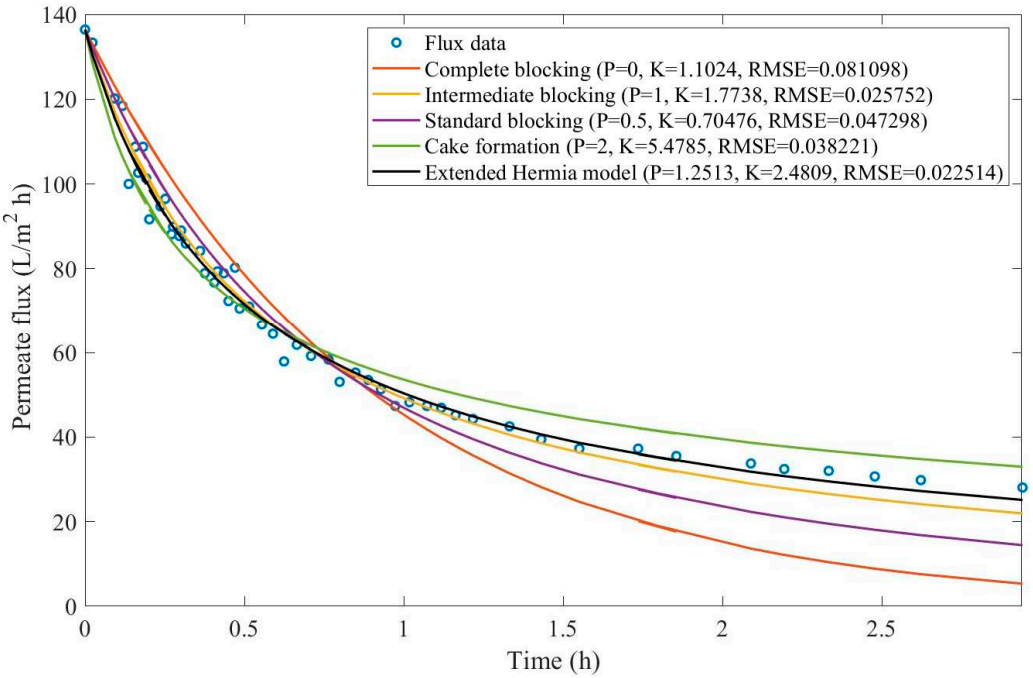

Figure D 10. Model fitting for corn syrup microfiltration with CM05 at 0.5 m/s and 50kPa considering the four original pore-blocking mechanisms and the extended Hermia model (16)

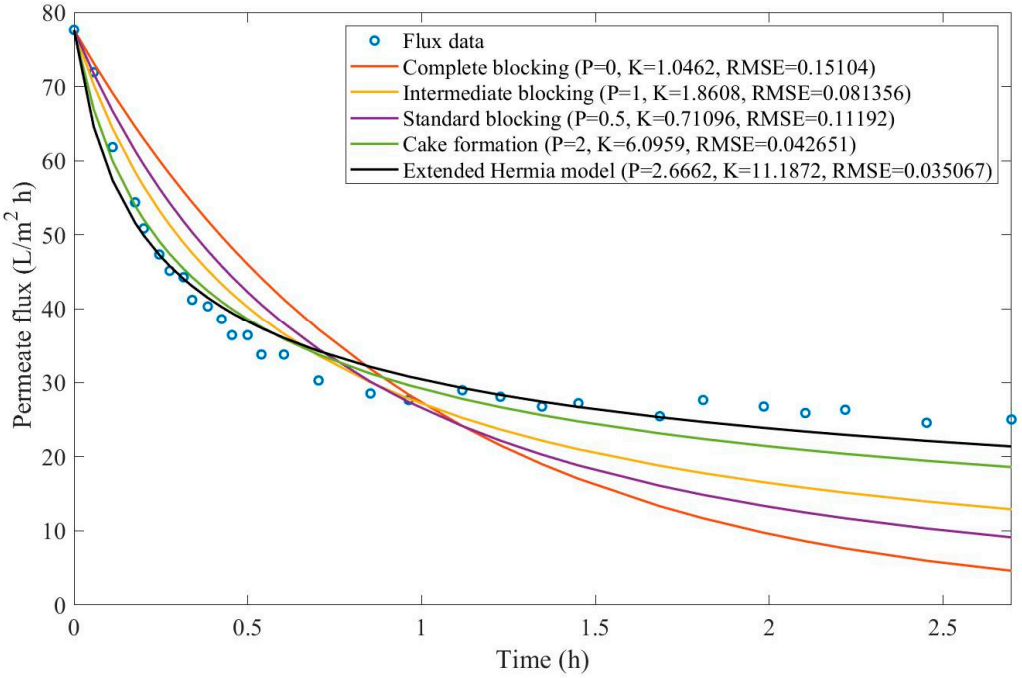

Figure D 11. Model fitting for corn syrup microfiltration with CM01 at 0.5 m/s and 50kPa considering the four original pore-blocking mechanisms and the extended Hermia model (16)

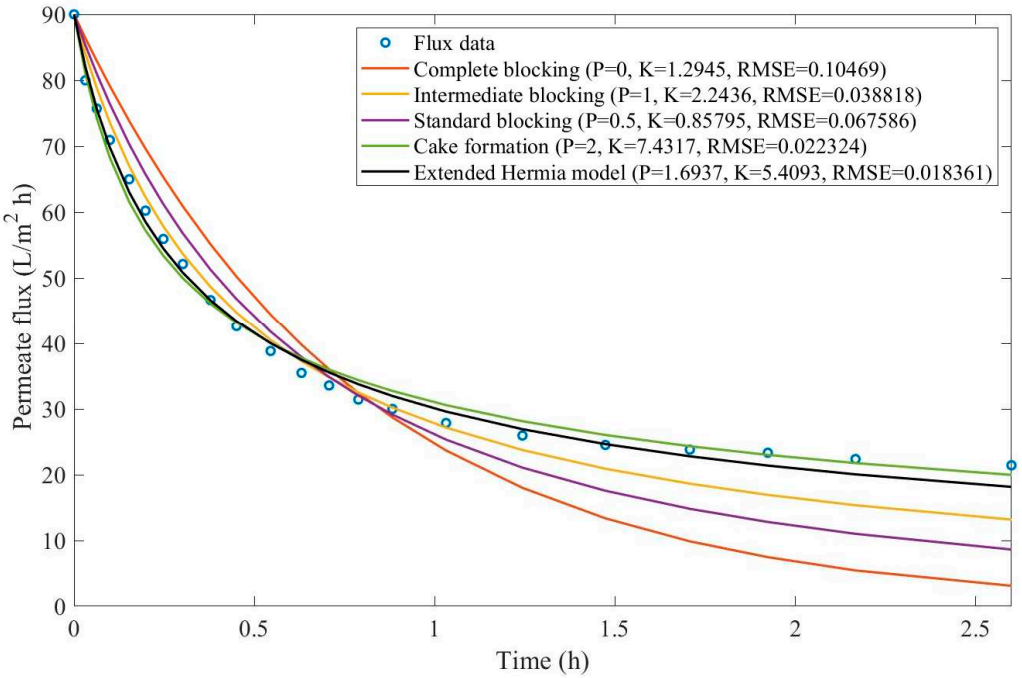

Figure D 12. Model fitting for corn syrup microfiltration with CM05 at 2.31 m/s and 37.9kPa considering the four original pore-blocking mechanisms and the extended Hermia model (16)

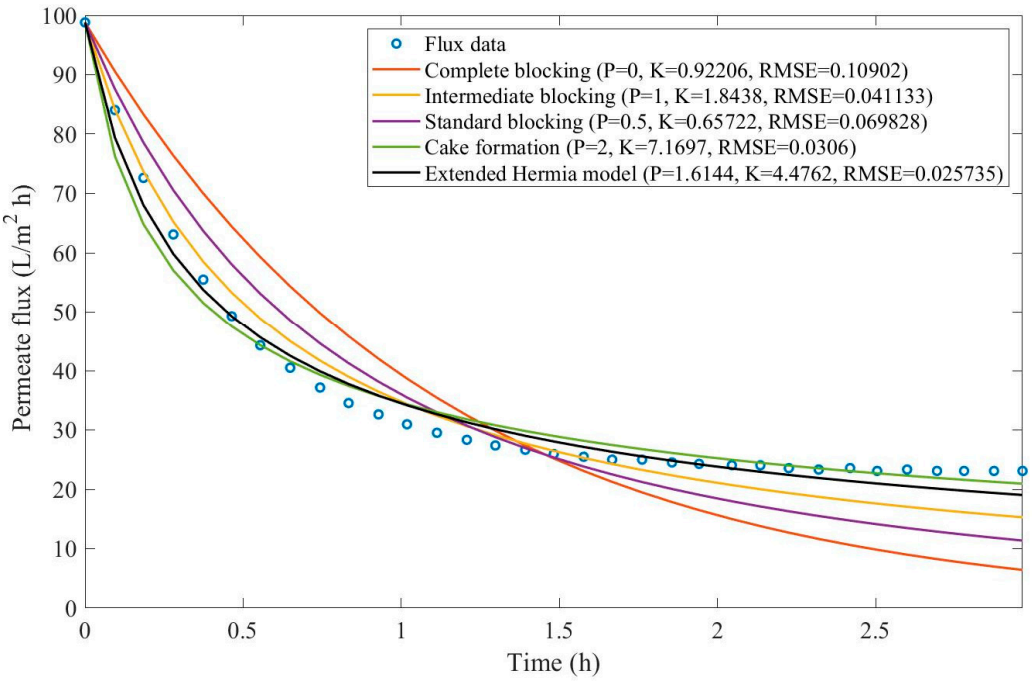

Figure D 13. Model fitting for corn syrup microfiltration with CM05 at 2.31 m/s and 51.71kPa considering the four original pore-blocking mechanisms and the extended Hermia model (16)

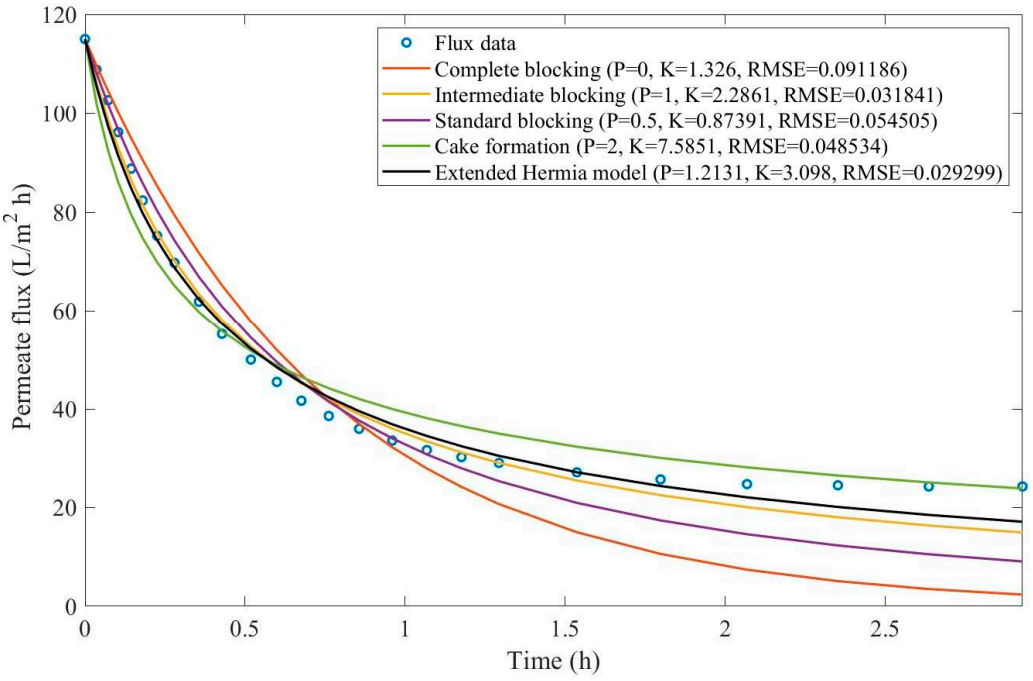

Figure D 14. Model fitting for corn syrup microfiltration with CM05 at 2.31 m/s and 103.42kPa considering the four original pore-blocking mechanisms and the extended Hermia model (16)

Example 3:

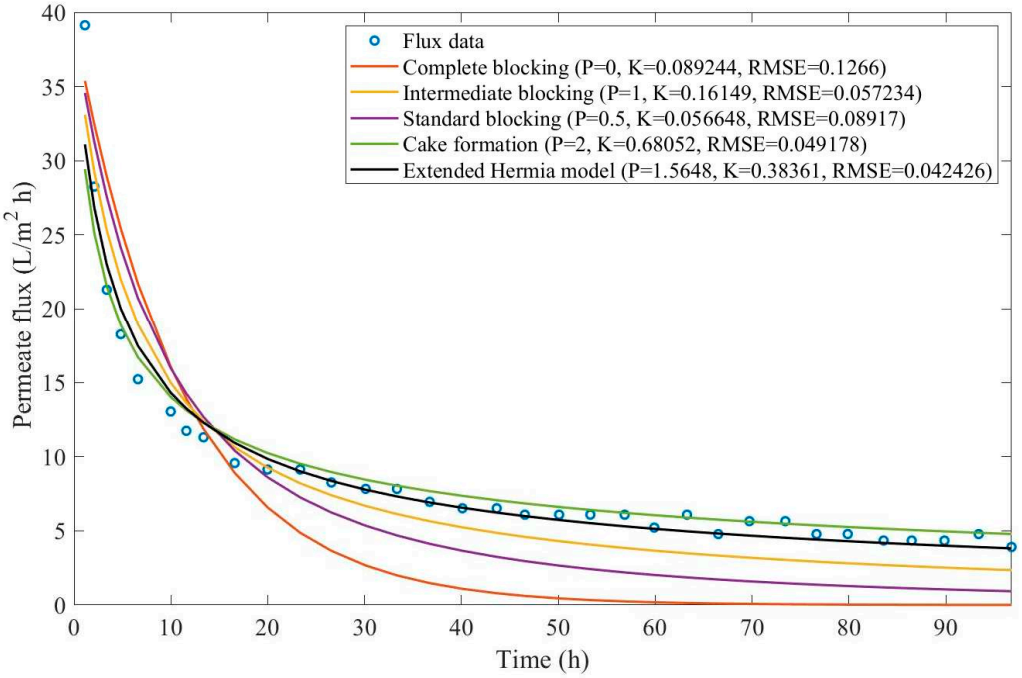

Figure D 15. Model fitting for oily effluent ultrafiltration with CFR of 14L/min and 21kPa considering the four original pore-blocking mechanisms and the extended Hermia model (17)

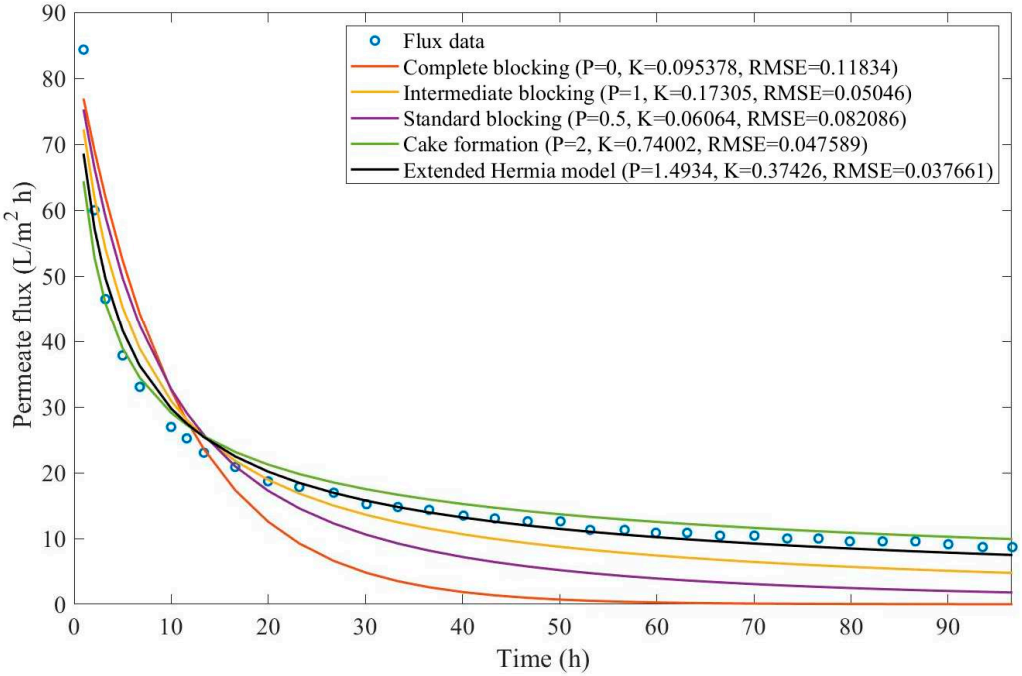

Figure D 16. Model fitting for oily effluent ultrafiltration with CFR of 14L/min and 35kPa considering the four original pore-blocking mechanisms and the extended Hermia model (17)

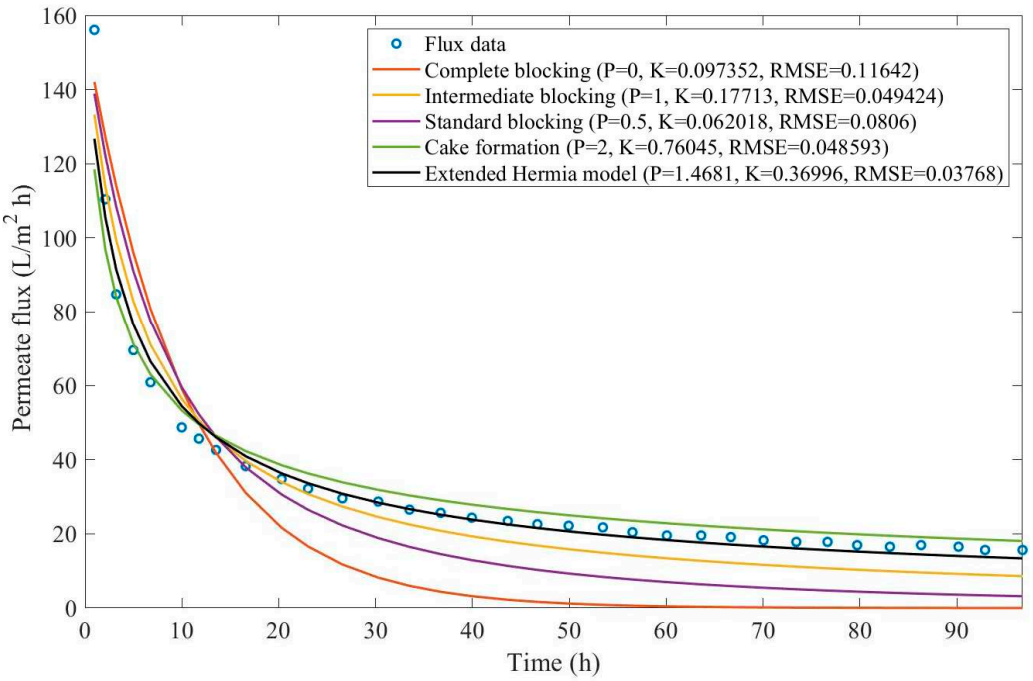

Figure D 17. Model fitting for oily effluent ultrafiltration with CFR of 14L/min and 104kPa considering the four original pore-blocking mechanisms and the extended Hermia model (17)

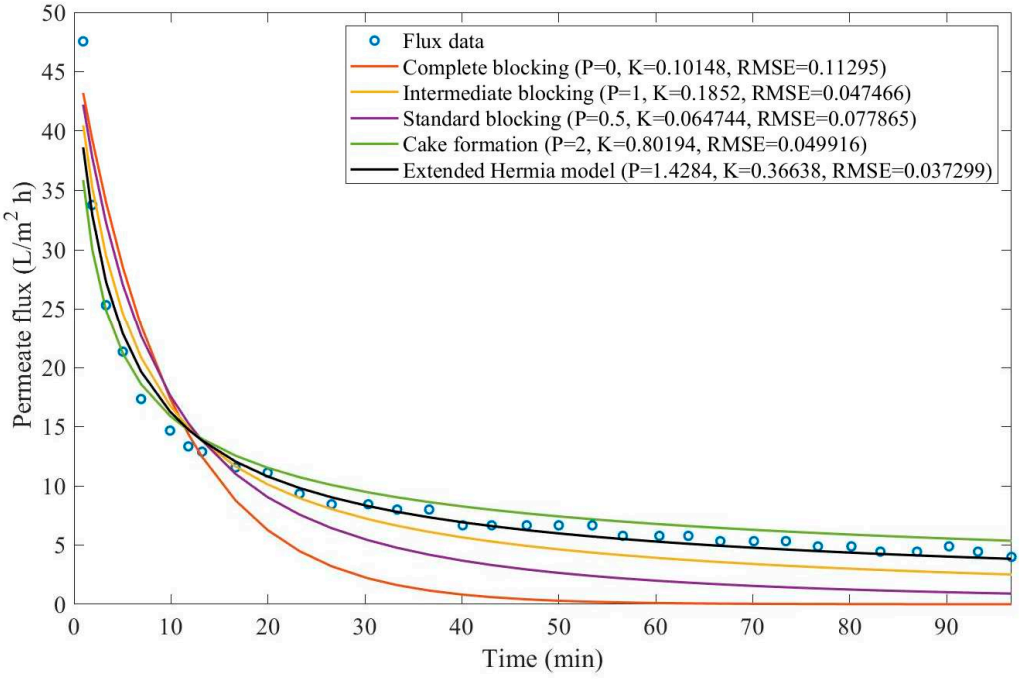

Figure D 18. Model fitting for oily effluent ultrafiltration with CFR of 28L/min and 21kPa considering the four original pore-blocking mechanisms and the extended Hermia model (17)

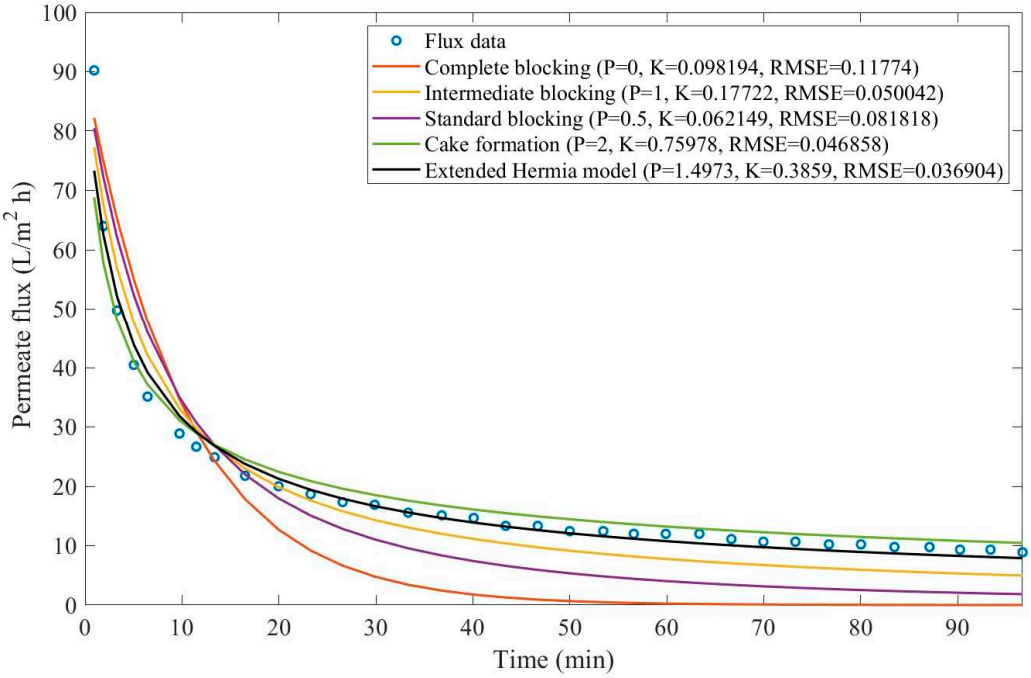

Figure D 19. Model fitting for oily effluent ultrafiltration with CFR of 28L/min and 35kPa considering the four original pore-blocking mechanisms and the extended Hermia model (17)

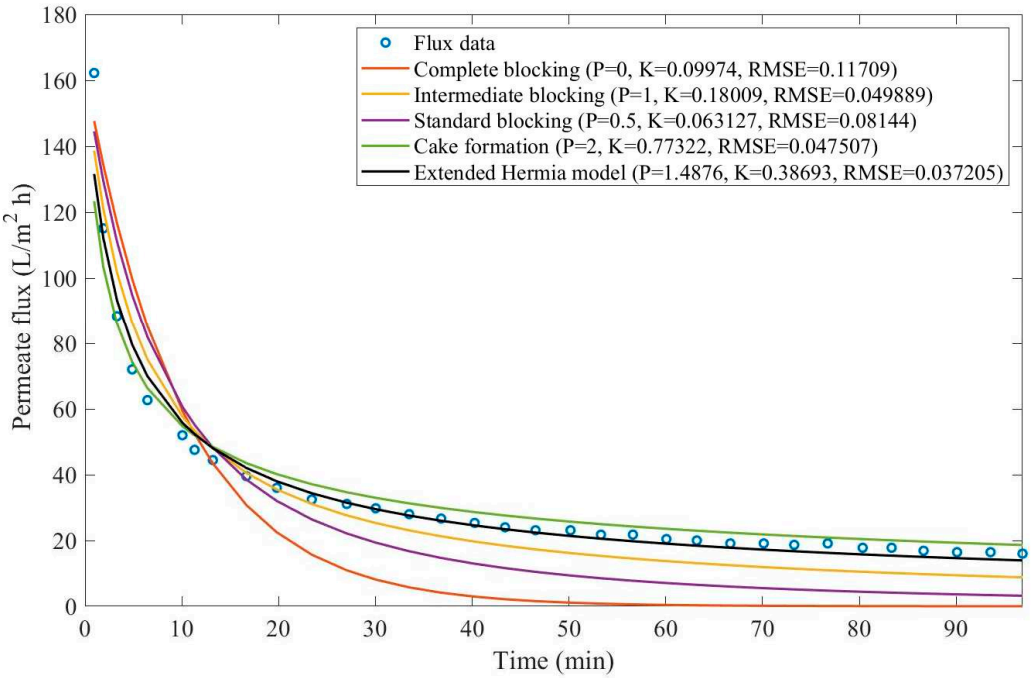

Figure D 20. Model fitting for oily effluent ultrafiltration with CFR of 28L/min and 104kPa considering the four original pore-blocking mechanisms and the extended Hermia model (17)

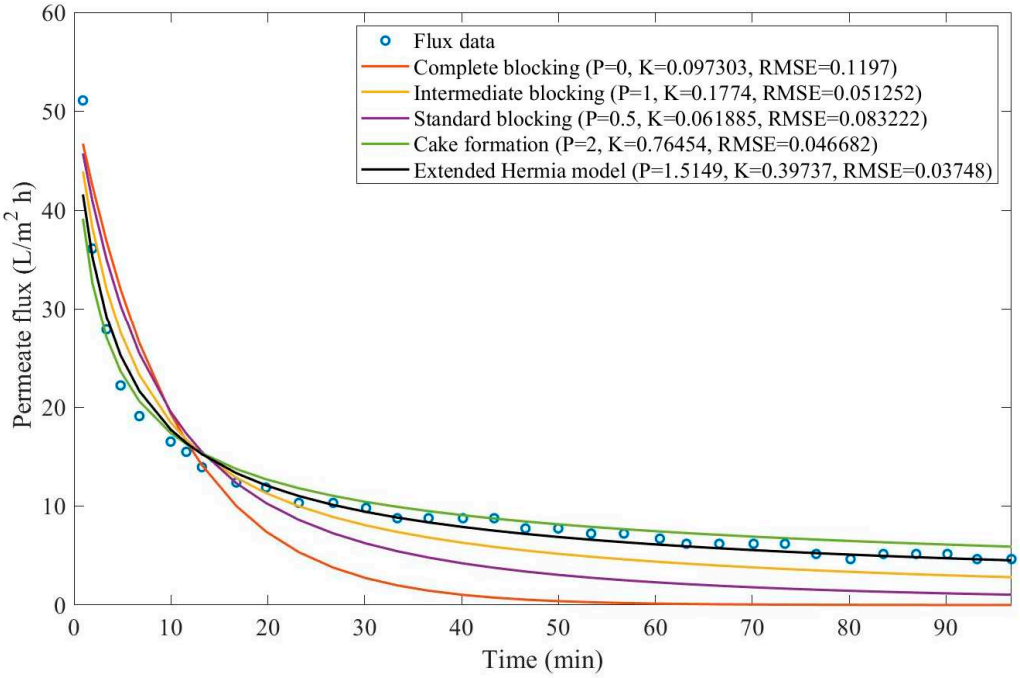

Figure D 21. Model fitting for oily effluent ultrafiltration with CFR of 40L/min and 21kPa considering the four original pore-blocking mechanisms and the extended Hermia model (17)

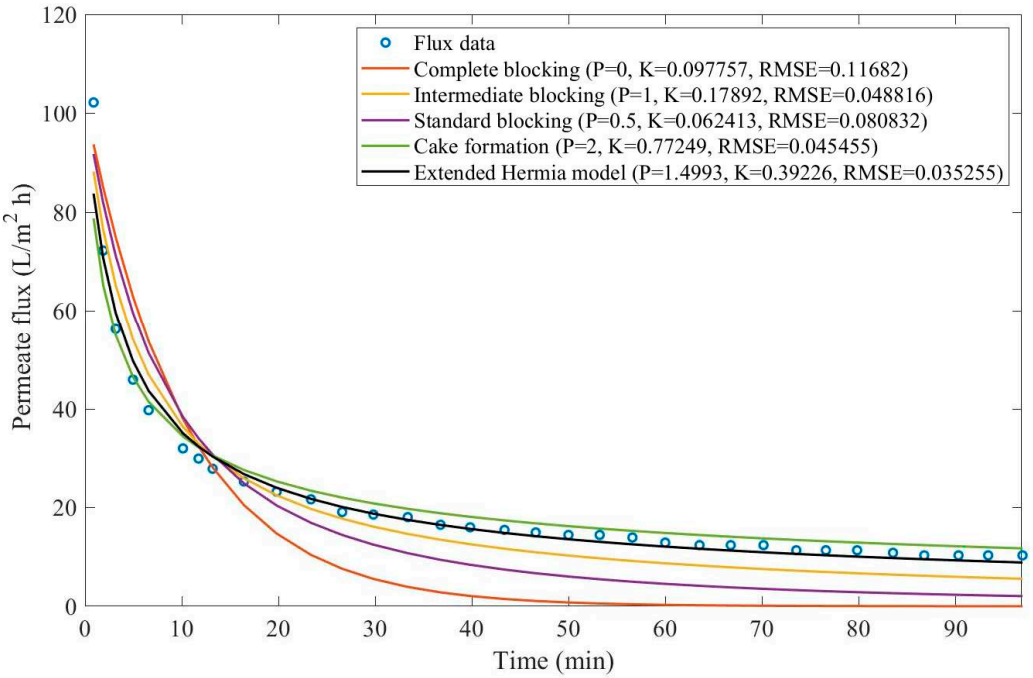

Figure D 22. Model fitting for oily effluent ultrafiltration with CFR of 40L/min and 35kPa considering the four original pore-blocking mechanisms and the extended Hermia model (17)

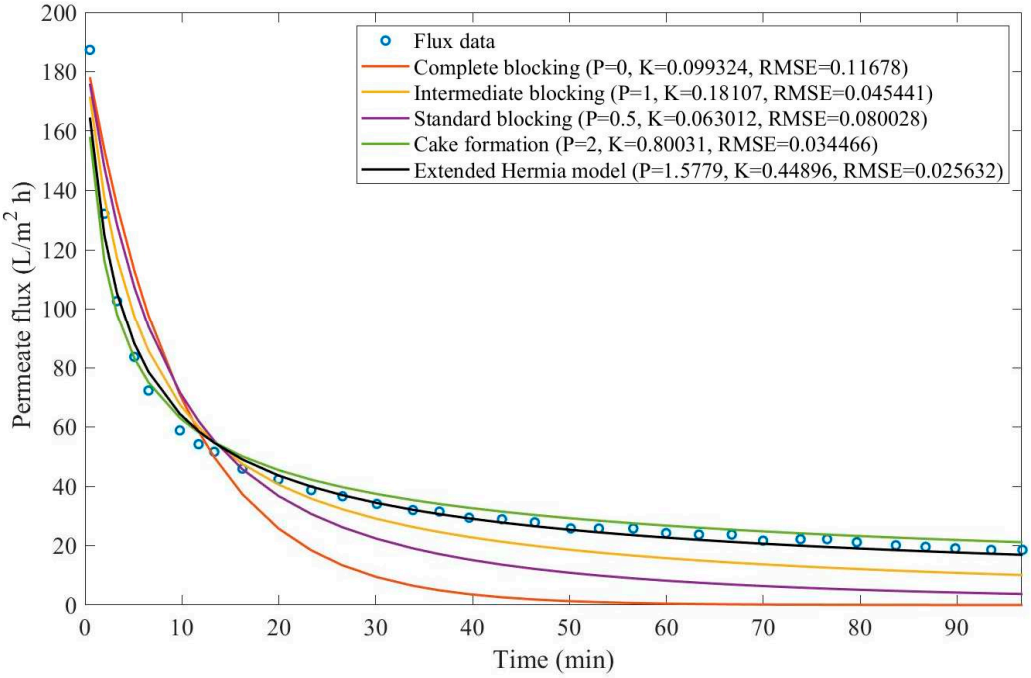

Figure D 23. Model fitting for oily effluent ultrafiltration with CFR of 40L/min and 104kPa considering the four original pore-blocking mechanisms and the extended Hermia model (17)

Example 4:

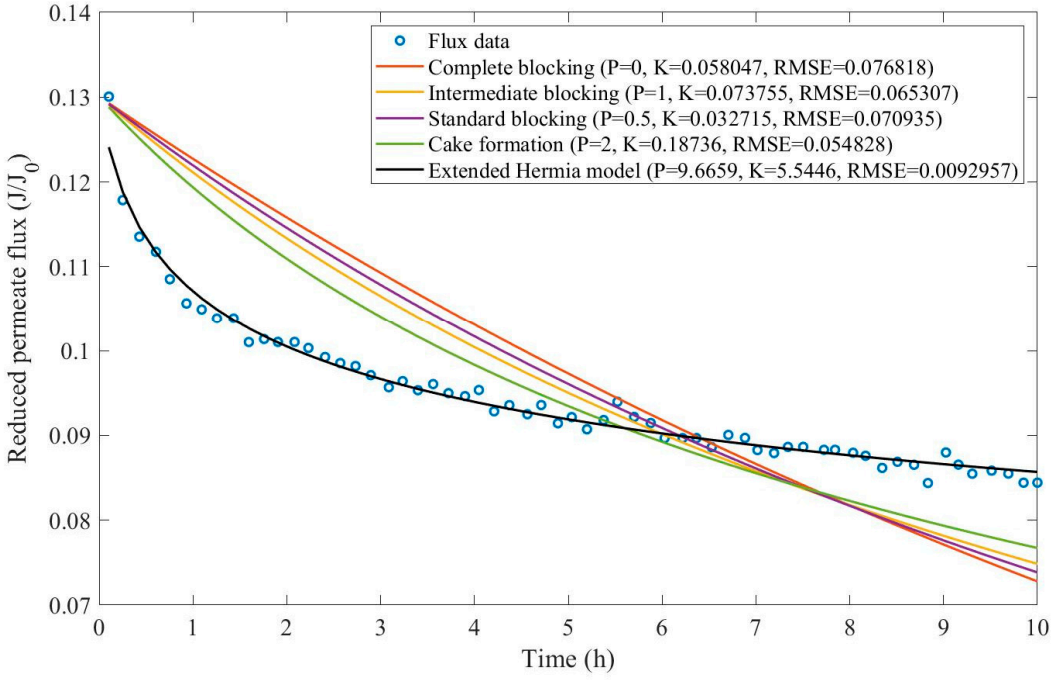

Figure D 24. Model fitting for ultrafiltration of flooding wastewater at 2.12bar and cross-flow velocity of 2.5m/s considering the four original pore blocking mechanisms and the extended Hermia model (18)

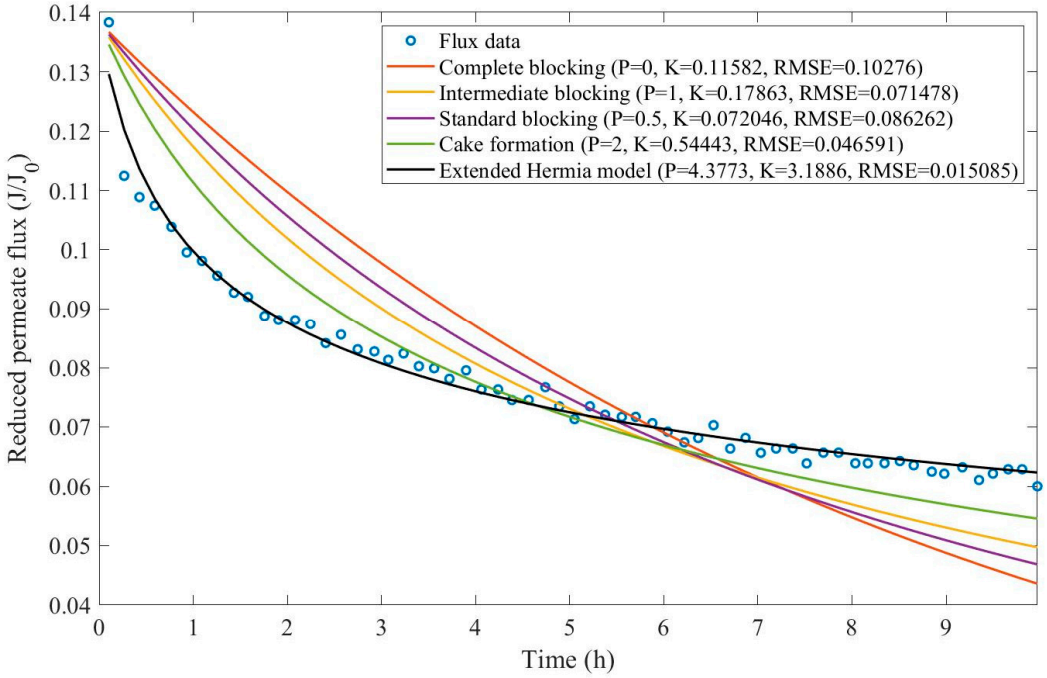

Figure D 25. Model fitting for ultrafiltration of flooding wastewater at 2.79bar and cross-flow velocity of 2.5m/s considering the four original pore blocking mechanisms and the extended Hermia model (18)

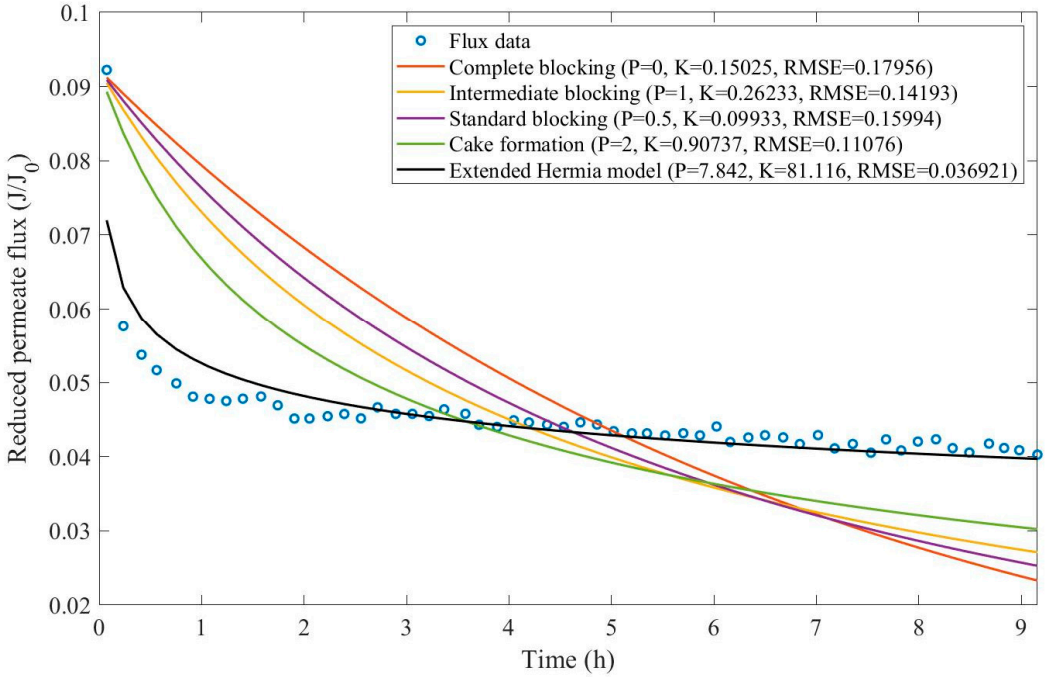

Figure D 26. Model fitting for ultrafiltration of flooding wastewater at 2.20bar and cross-flow velocity of 0.75m/s considering the four original pore blocking mechanisms and the extended Hermia model (18)

Preprints (www.preprints.org) | NOT PEER-REVIEWED | Posted: 5 January 2023 doi:10.20944/preprints202206.0187.v2

Peer-reviewed version available at Membranes 2023, 13, 290; doi:10.3390/membranes13030290

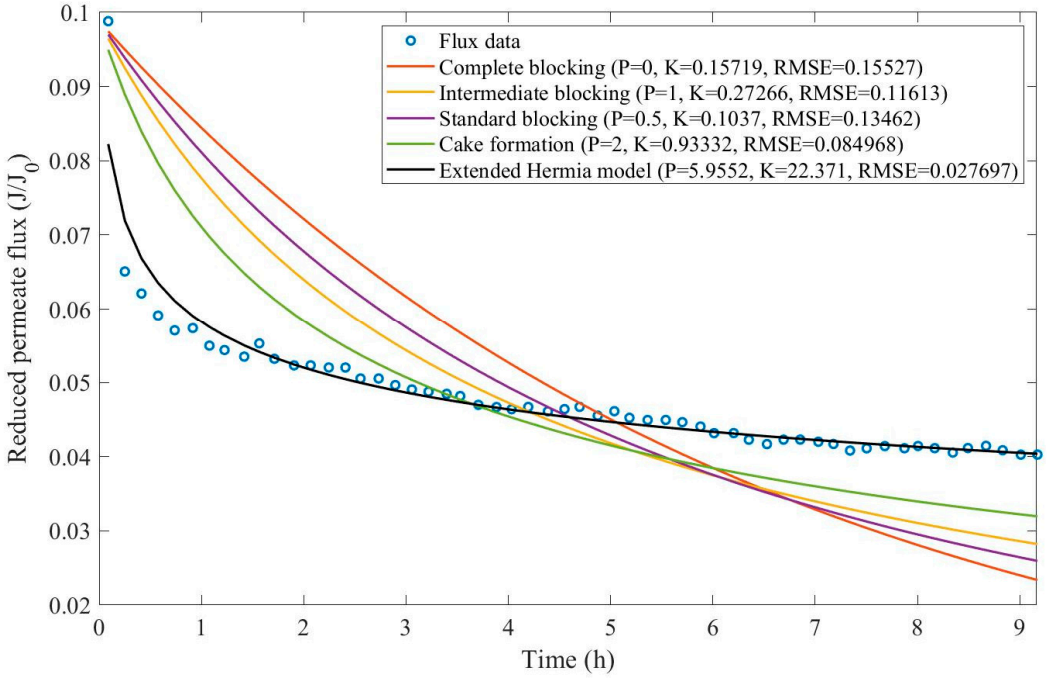

Figure D 27. Model fitting for ultrafiltration of flooding wastewater at 2.20bar and cross-flow velocity of 1.50m/s considering the four original pore blocking mechanisms and the extended Hermia model (18)

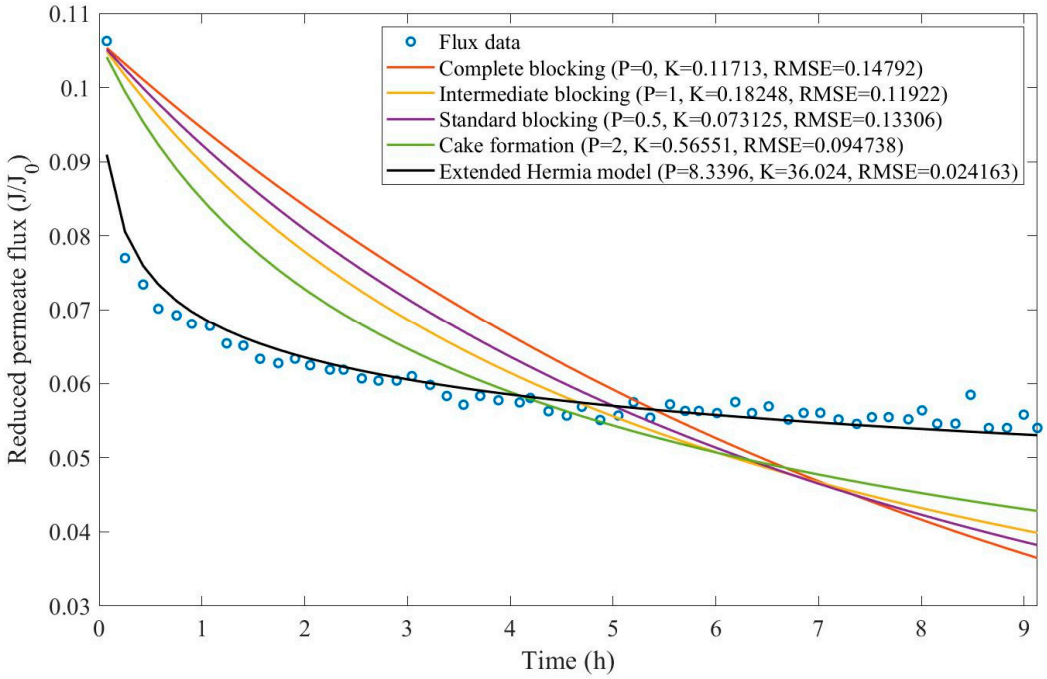

Figure D 28. Model fitting for ultrafiltration of flooding wastewater at 2.20bar and cross-flow velocity of 2.25m/s considering the four original pore blocking mechanisms and the extended Hermia model (18)

Preprints (www.preprints.org) | NOT PEER-REVIEWED | Posted: 5 January 2023 doi:10.20944/preprints202206.0187.v2

Peer-reviewed version available at Membranes 2023, 13, 290; doi:10.3390/membranes13030290

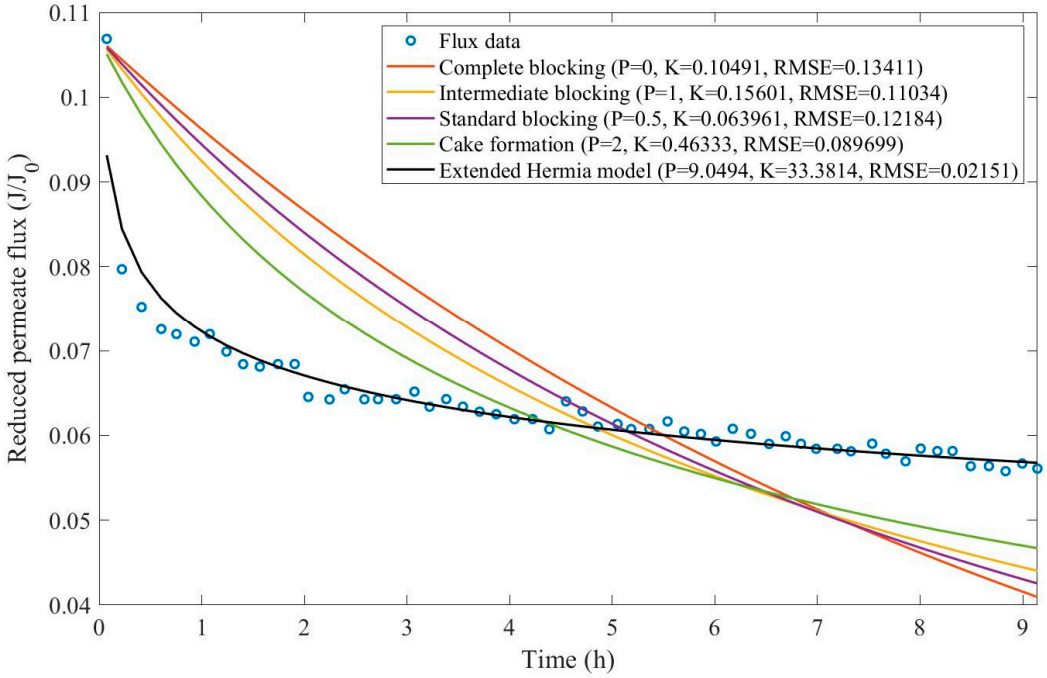

Figure D 29. Model fitting for ultrafiltration of flooding wastewater at 2.20bar and cross-flow velocity of 3.00m/s considering the four original pore blocking mechanisms and the extended Hermia model (18)

Example 5:

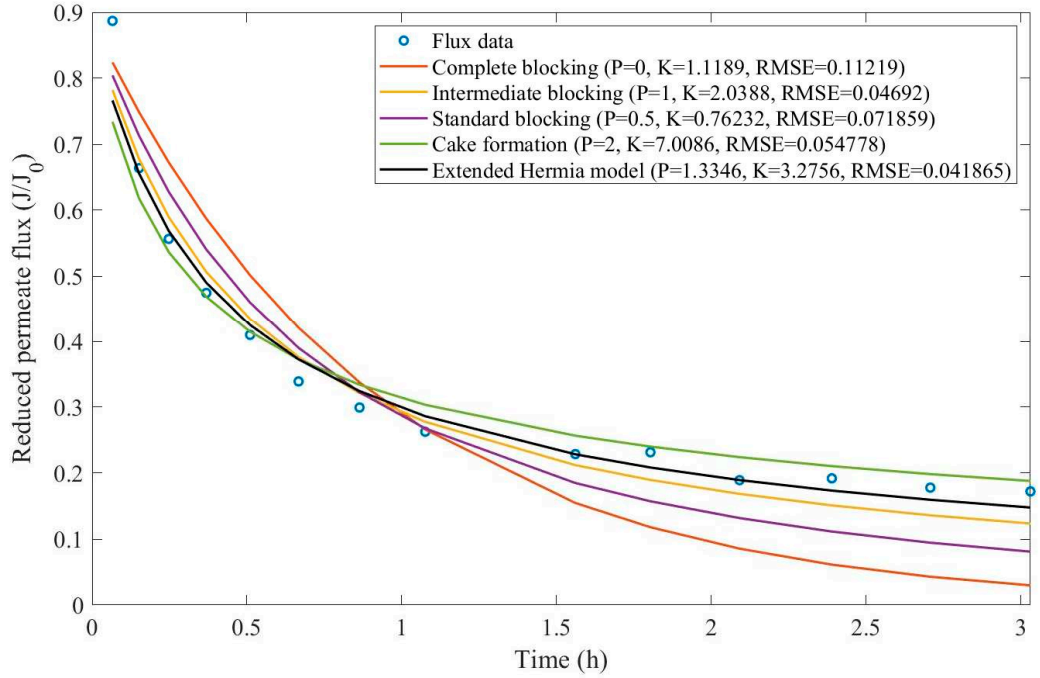

Figure D 30. Model fitting for the first fouling stage of ultrafiltration of bovine serum albumin solution at 103.421kPa considering the four original pore-blocking mechanisms and the extended Hermia model (Uncoated membrane) (19)

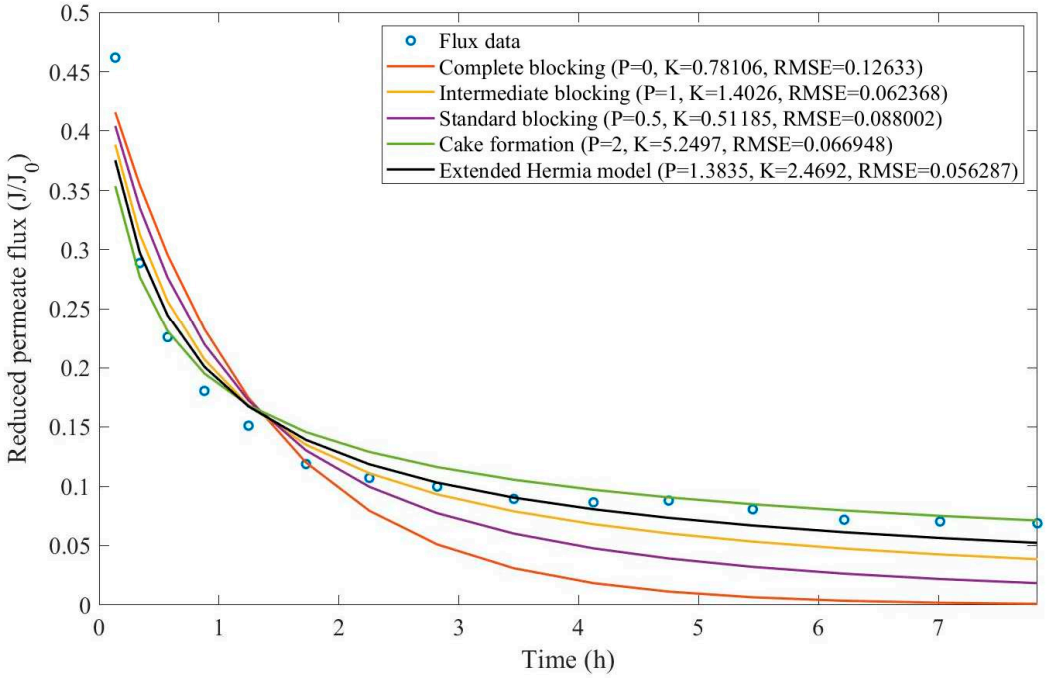

Figure D 31. Model fitting for the second fouling stage of ultrafiltration of bovine serum albumin solution at 103.421kPa considering the four original pore-blocking mechanisms and the extended Hermia model (Uncoated membrane) (19)

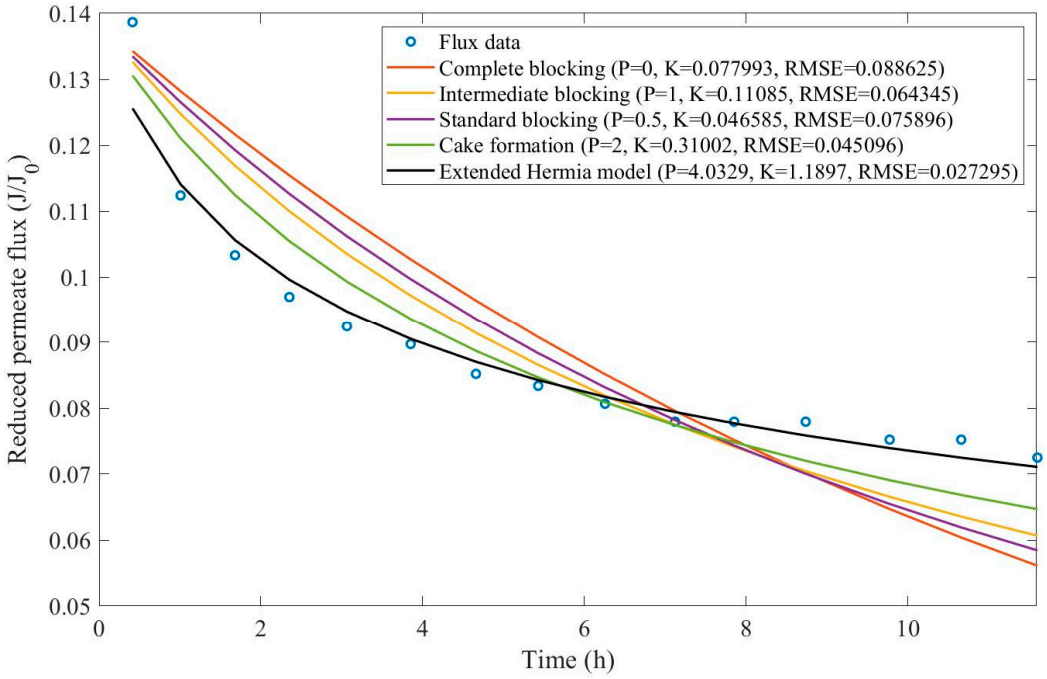

Figure D 32. Model fitting for the third fouling stage of ultrafiltration of bovine serum albumin solution at 103.421kPa considering the four original pore-blocking mechanisms and the extended Hermia model (Uncoated membrane) (19)

Preprints (www.preprints.org) | NOT PEER-REVIEWED | Posted: 5 January 2023 doi:10.20944/preprints202206.0187.v2

Peer-reviewed version available at Membranes 2023, 13, 290; doi:10.3390/membranes13030290

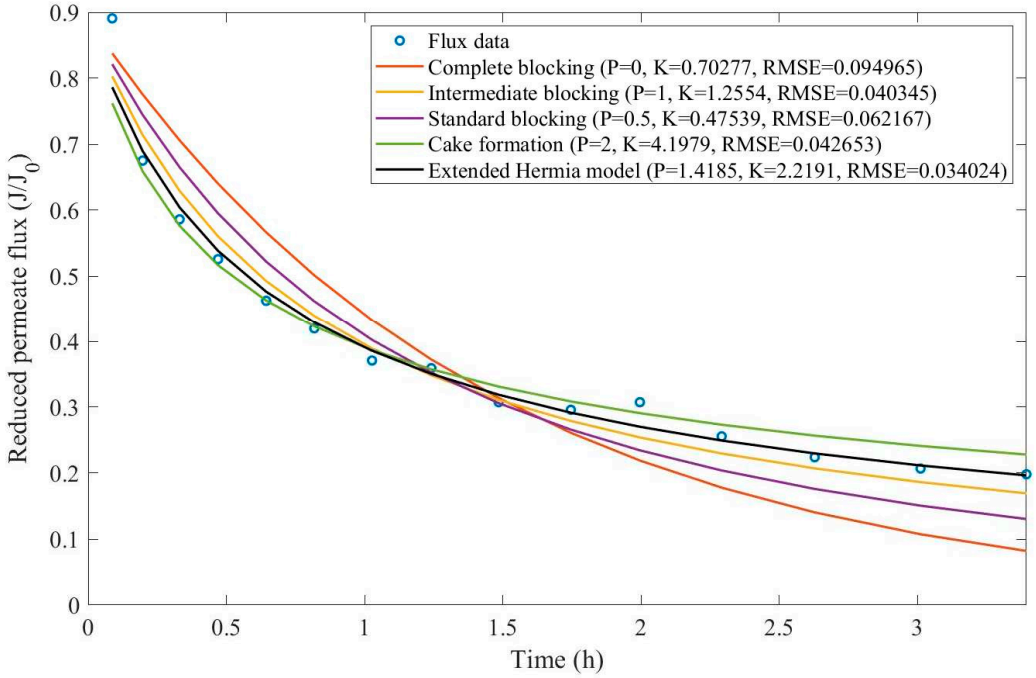

Figure D 33. Model fitting for the first fouling stage of ultrafiltration of bovine serum albumin solution at 103.421kPa considering the four original pore-blocking mechanisms and the extended Hermia model (Coated membrane) (19)

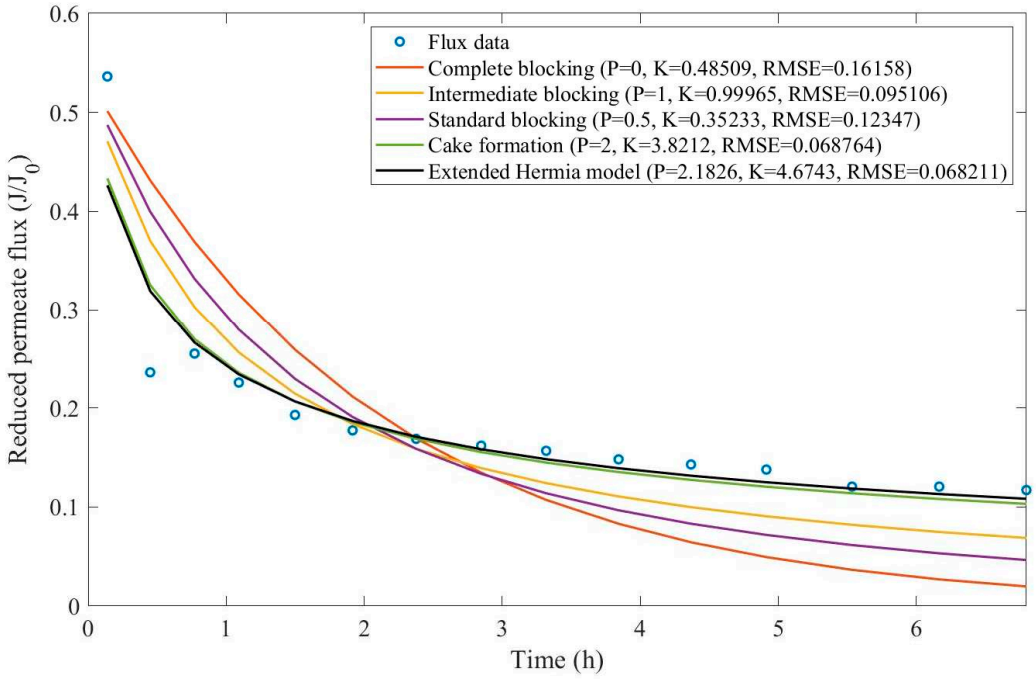

Figure D 34. Model fitting for the second fouling stage of ultrafiltration of bovine serum albumin solution at 103.421kPa considering the four original pore-blocking mechanisms and the extended Hermia model (Coated membrane) (19)

Preprints (www.preprints.org) | NOT PEER-REVIEWED | Posted: 5 January 2023 doi:10.20944/preprints202206.0187.v2

Peer-reviewed version available at Membranes 2023, 13, 290; doi:10.3390/membranes13030290

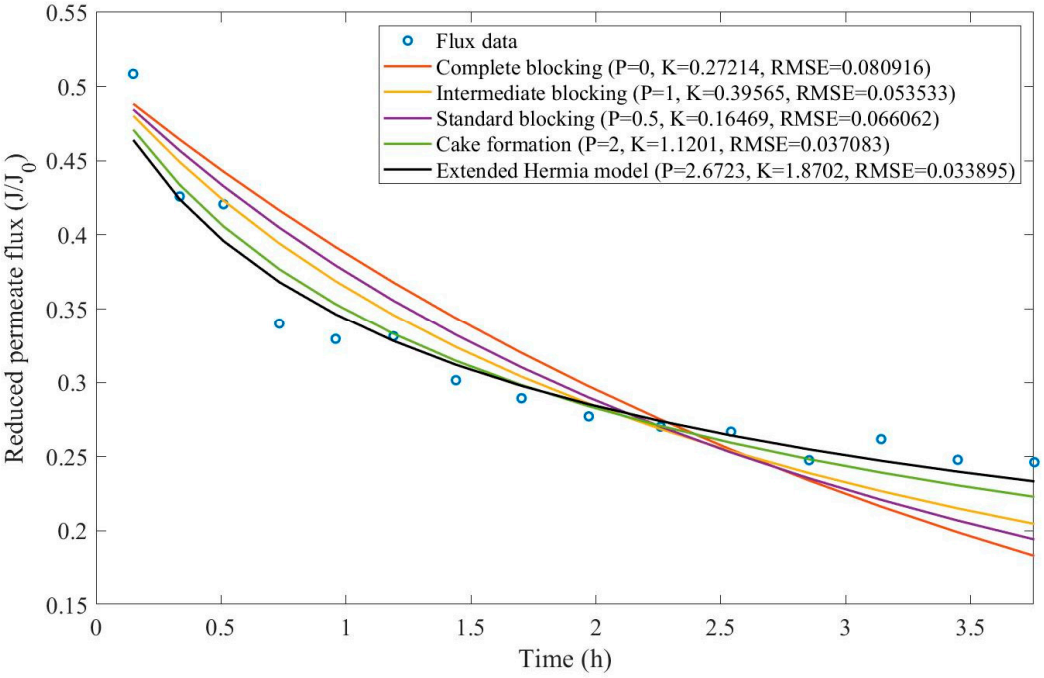

Figure D 35. Model fitting for the third fouling stage of ultrafiltration of bovine serum albumin solution at 103.421kPa considering the four original pore-blocking mechanisms and the extended Hermia model (Coated membrane) (19)

Example 6:

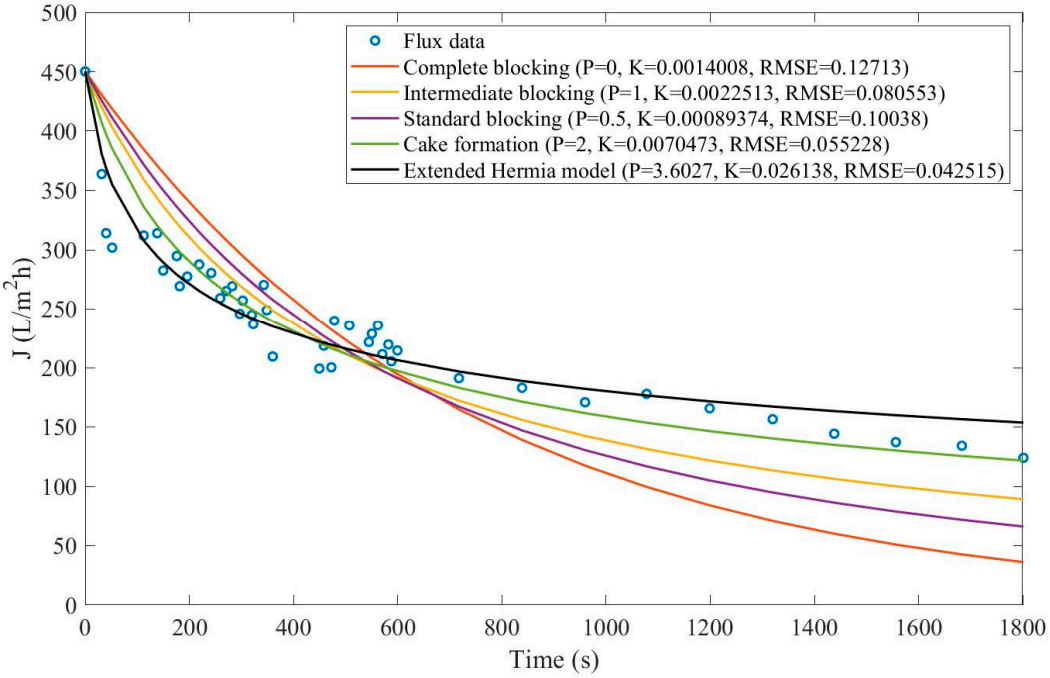

Figure D 36. Model fitting for dead-end ultrafiltration of nanoparticles (97mgNPs/L) from polishing wastewater at 0.4bar considering the four original pore-blocking mechanisms and the extended Hermia model (20)

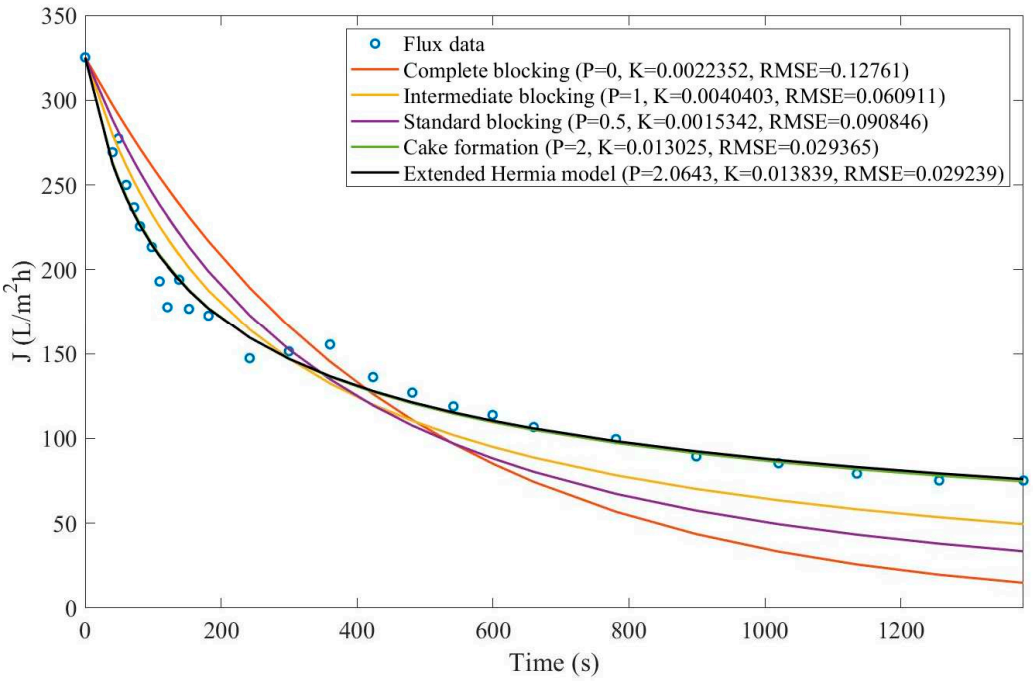

Figure D 37. Model fitting for dead-end ultrafiltration of nanoparticles (251mgNPs/L) from polishing wastewater at 0.4bar considering the four original pore-blocking mechanisms and the extended Hermia model (20)

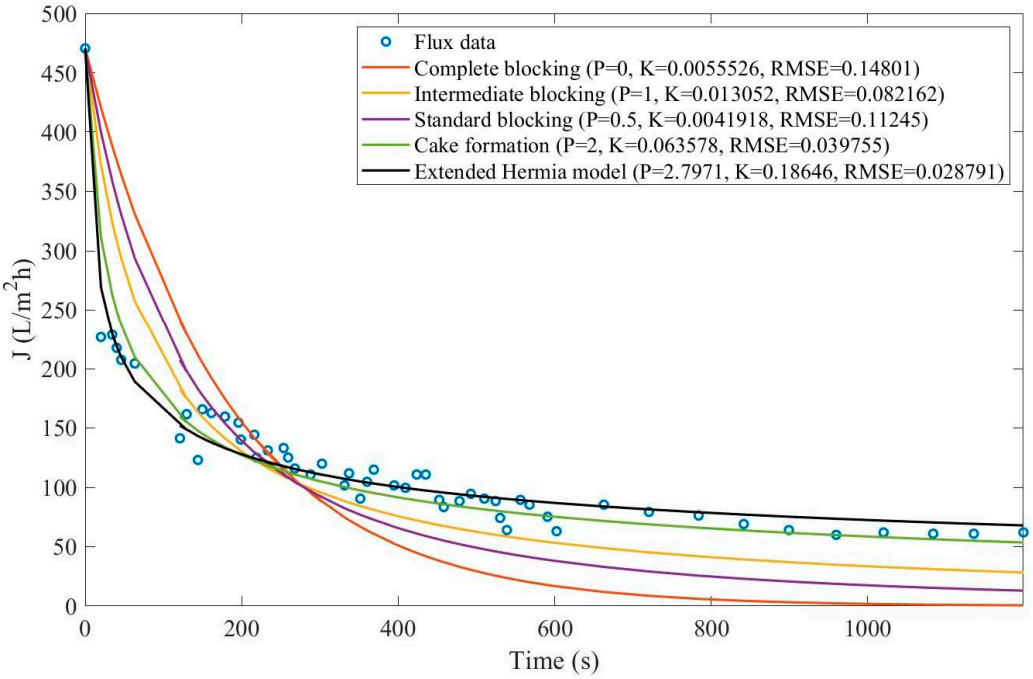

Figure D 38. Model fitting for dead-end ultrafiltration of nanoparticles (657mgNPs/L) from polishing wastewater at 0.4bar considering the four original pore-blocking mechanisms and the extended Hermia model (20)

References

1. Hermia, J. Constant pressure blocking filtration laws—application to power-law non-newtonian fluids, Trans. Inst. Chem. Eng. 60 (1982) 183–187.
2. Vela, M., Blanco, S., García, J. and Rodríguez, E. Analysis of membrane pore blocking models applied to the ultrafiltration of PEG, Separation and Purification Technology 62 (2008) 489–498, doi: 10.1016/j.seppur.2008.02.028
3. Kurada, K., Tanmay and De, S. Modeling of cross flow hollow fiber ultrafiltration for treatment of effluent from Railway Workshop, Journal of Membrane Science 551 (2018) 223–233, doi: 10.1016/j.memsci.2018.01.051
4. Li, S., Luo, J., Hang, X., Zhao, S. and Wan, Y. Removal of polycyclic aromatic hydrocarbons by nanofiltration membranes: Rejection and fouling mechanisms, Journal of Membrane Science 582 (2019) 264–273, doi: 10.1016/j.memsci.2019.04.008
5. Gomes, M., Arroyo, P. and Pereira, N. Biodiesel production from degummed soybean oil and glycerol removal using ceramic membrane, Journal of Membrane Science 378 (2011) 453–461, doi: 10.1016/j.memsci.2011.05.033
6. Gomes, M., Arroyo, P. and Pereira, N. Influence of acidified water addition on the biodiesel and glycerol separation through membrane technology, Journal of Membrane Science 431 (2013) 28–36, doi: 10.1016/j.memsci.2012.12.036
7. Chang, E., Yang, S., Huang, C., Liang, C. and Chiang, P. Assessing the fouling mechanisms of high-pressure nanofiltration membrane using the modified Hermia model and the resistance-in-series model, Separation and Purification Technology 79 (2011) 329–336, doi: 10.1016/j.seppur.2011.03.017
8. Hasyimah, M. and Mohammad, A. Assessment of Fouling Mechanisms in Treating Organic Solutes Synthesizing Glycerin−Water Solutions by Modified Hermia Model, Industrial and Engineering Chemistry Research 53 (2014) 15213−15221, doi: 10.1021/ie502509d
9. Pan, Y., Wang, W., Wang, T. and Yao, P. Fabrication of carbon membrane and microfiltration of oil-in-water emulsion: An investigation on fouling mechanisms, Separation and Purification Technology 57 (2007) 388–393, doi: 10.1016/j.seppur.2007.04.024
10. Jegatheesan, V., Phong, D. D., Shu, L., & Ben Aim, R. (2009). Performance of ceramic micro- and ultrafiltration membranes treating limed and partially clarified sugar cane juice. Journal of Membrane Science, 327(1-2), 69–77. doi:10.1016/j.memsci.2008.11.008
11. Çengel, Y. and Cimbala, J. Fluid Mechanics: Fundamentals and Applications, 1st Edition by McGraw-Hill Higher Education. ISBN: 0-07-247236-7.
12. Welty, J., Rorrer, G. and Foster, D. Fundamentals of Momentum, Heat, and Mass Transfer, 6th Edition by John Wiley & Sons, Inc. ISBN: 978-0-470-50481-9.
13. Magyar, P. Derivative of Inverse Functions, Lecture notes. Available at [https://users.math.msu.edu/users/magyarp/]. Accessed at 11/06/2021.
14. Protter, M., Morrey, C. Intermediate Calculus: Differentiation under the Integral Sign, 2nd Edition by Springer. ISBN: 978-0-387-96058-6.
15. Jung, C. and Son, H. Evaluation of membrane fouling mechanism in various membrane pretreatment processes, Desalination and Water Treatment, 2:1-3, 199-208, doi: 10.5004/dwt.2009.256
16. Almandoz, C., Pagliero, C., Ochoa, A. and Marchese, J. Corn syrup clarification by microfiltration with ceramic membranes, Journal of Membrane Science 363 (2010) 87-95, doi: 10.1016/j.memsci.2010.07.017
17. Kurada, K. and Tanmay, S. Modeling of cross flow hollow fiber ultrafiltration for treatment of effluent from Railway Workshop, Journal of Membrane Science 551 (2018) 223-233, doi: 10.1016/j.memsci.2018.01.051
18. Ren, L., Yu, S., Li, J. and Li, L. Pilot study on the effects of operating parameterson membrane fouling during ultrafiltration ofalkali/surfactant/polymerflooding wastewater:optimization and modeling, RSCAdv.,2019,9, 11111–11122. doi: 10.1039/c8ra10167a
19. Storms, M., Kadhem, A., Xiang, S., Bernards, M., Gentile, G. and Cortalezzi, M. Enhancement of the fouling resistance of zwitterion coated ceramic membranes, Membranes 2020, 10, 210, doi: 10.3390/membranes10090210
20. Ohanessian, K., Monnot, M., Moulin, P., Ferrasse, J., Barca, C., Soric, A. and Boutin, O. Dead-end and crossflow ultrafiltration process modelling: application on chemical mechanical polishing wastewaters, Chemical Engineering Research and Design, 2020, 158, 164-176, doi: 10.1016/j.cherd.2020.04.007